Thesis for the Degree of Doctor of Philosophy

Multilevel Modulation and Transmission in VCSEL-based Short-range Fiber Optic Links

Tamás Lengyel

Photonics Laboratory
Department of Microtechnology and Nanoscience (MC2)
Chalmers University of Technology
Göteborg, Sweden, 2019

Multilevel Modulation and Transmission in VCSEL-based Short-range Fiber Optic Links

Tamás Lengyel

Göteborg, April 2019

© Tamás Lengyel, 2019

ISBN 978-91-7905-107-5

Doktorsavhandlingar vid Chalmers Tekniska Högskola
Ny serie 4574
ISSN 0346-718X

Technical Report MC2-412
ISSN 1652-0769

Chalmers University of Technology
Department of Microtechnology and Nanoscience (MC2)
Photonics Laboratory
Chalmers University of Technology, SE-412 96 Göteborg, Sweden
Phone: +46 (0) 31 772 1000

Front cover illustration: A high-speed VCSEL fabricated at Chalmers with modulating signals below (OOK with pre-emphasis, 3-PAM, 4-PAM) and the captured optical signals emitted by the VCSEL above.

Printed by Chalmers reproservice, Chalmers University of Technology
Göteborg, Sweden, April, 2019

Multilevel Modulation and Transmission in VCSEL-based Short-range Fiber Optic Links

Tamás Lengyel

Chalmers University of Technology
Department of Microtechnology and Nanoscience (MC2)
Photonics Laboratory, SE-412 96 Göteborg, Sweden

Abstract

As the demand for ever higher throughput short-range optical links is growing, research and industry associations have shown increased interest in multilevel modulation formats, such as the four leveled pulse amplitude modulation, referred to as 4-PAM. As on-off keying (OOK) persists to be the choice for low latency applications, for example high performance computing, datacenter operators see 4-PAM as the next format to succeed current OOK-based optical interconnects. Throughput can be increased in many ways: parallel links can be deployed, multicore fibers can be used or more efficient modulation formats with digital signal processing is an alternative. Therefore, to improve link data rates, the introduction of new modulation formats and pre-emphasis are primarily considered in this thesis.

In a bandwidth-limited link, turning towards spectrally efficient formats is one of the methods to overcome the bandwidth requirements of OOK. Such are the considerations when opting for 3-PAM or 4-PAM schemes. Both require lower bandwidth than OOK and are potential candidates in such scenarios. 4-PAM provides double spectral efficiency and double data rate at the same symbol rate as on-off keying, but, as with any technology transition, new challenges emerge, such as a higher SNR requirement, a lower tolerance to VCSEL nonlinearities and skewing of the signal in the time domain. 3-PAM could potentially be an in-between solution, as it requires 33% less bandwidth than OOK and is less sensitive to VCSEL dynamics which could impair the transmission. A study is presented where 3-PAM has outperformed both OOK and 4-PAM in the same link. Detailed investigation of legacy 25G class VCSELs has shown that devices with moderate damping are suitable for the transition to 4-PAM.

The pre-emphasis of signals is a powerful tool to increase link bandwidth at the cost of modulation amplitude. This has been investigated in this thesis for on-off keying and has shown 9% and 27% increase in bit rate for error-free operation with two pre-emphasis approaches. Similarly, pre-emphasis of a 4-PAM electrical signals has enabled 71.8 Gbps transmission back-to-back with lightweight forward error correction and 94 Gbps net data rate was achieved with the same pre-emphasis and post-processing using an offline least-mean-square equalizer.

Keywords: Data communication, vertical cavity surface emitting lasers, intensity modulation, multimode fiber, NRZ OOK, 3-PAM, 4-PAM, IM/DD, optical interconnects, short-range fiber optic links, inter-symbol interference

List of papers

This thesis is based on the following appended papers:

[A] **T. Lengyel**, K. Szczerba, P. Westbergh, M. Karlsson, A. Larsson, and P. A. Andrekson, "Sensitivity Improvements in an 850 nm VCSEL-based Link using a Two-tap Pre-emphasis Electronic Filter," *Journal of Lightwave Technology*, vol. 45, no. 9, pp. 1633-1639, 2017.

[B] **T. Lengyel**, K. Szczerba, M. Karlsson, A. Larsson, and P. A. Andrekson, "Demonstration of a 71.8 Gbps 4-PAM 850 nm VCSEL-based Link with a Pre-emphasizing Passive Filter," in Proceedings of the *42nd European Conference on Optical Communications*, Sept. 2016, paper Th.2.P2.SC4.6

[C] K. Szczerba, **T. Lengyel**, M. Karlsson, P. A. Andrekson, and A. Larsson, "94-Gb/s 4-PAM Using an 850-nm VCSEL, Pre-Emphasis, and Receiver Equalization," *Photonics Technology Letters*, vol. 28, no. 22, 2016.

[D] **T. Lengyel**, K. Szczerba, Emanuel P. Haglund, P. Westbergh, M. Karlsson, A. Larsson, and P. A. Andrekson, "Impact of Damping on 50 Gbps 4-PAM Modulation of 25G Class VCSELs," *Journal of Lightwave Technology*, vol. 35, no. 19, pp. 4203-4209, 2017.

[E] **T. Lengyel**, E. Simpanen, J. Gustavsson, A. Larsson, M. Karlsson, P. A. Andrekson, W. V. Sorin, S. Mathai, M. R. Tan and S. Bickham, "Pre-emphasis enabled 50 Gbit/s transmission over 1000 m SMF using a 1060 nm single-mode VCSEL," *Electronics Letters*, vol. 54, no. 20, pp. 1186 - 1187, 2018.

[F] **T. Lengyel**, M. Karlsson, E. Agrell, A. Larsson, and P. A. Andrekson "Investigation of 3-PAM transmission in a 850 nm VCSEL-based link," *submitted to Optics Express*

Related publications and conference contributions by the author not included in the thesis:

[G] I. C. Sezgin, J. Gustavsson, **T. Lengyel**, T. Eriksson, Z. S. He and C. Fager "Effect of VCSEL Characteristics on Ultra-High Speed Sigma-Delta-over-Fiber Communication Links," *Journal of Lightwave Technology, Early Access, 2019*

[H] K. Szczerba, **T. Lengyel**, Z. S. He, J. Chen, P. A. Andrekson, M. Karlsson, H, Zirath, A. G. Larsson "High-speed optical interconnects with 850nm VCSELS and advanced modulation formats," *Proceedings of SPIE*, vol. 10122, 101220G, 2017.

[I] E. Simpanen, J.S. Gustavsson, E. Haglund, E.P. Haglund, **T. Lengyel**, A. Larsson, P.A. Andrekson, W.V Sorin, S. Mathai, M. Tan, and S. Bickham "1060 nm single and multimode VCSELs for up to 50 Gb/s modulation," presented at *2017 IEEE Photonics Conference (IPC)*, Orlando, FL, USA, Oct. 2017.

[J] A. Larsson, J.S. Gustavsson, E. Haglund, E.P. Haglund, **T. Lengyel**, E. Simpanen and M. Jahed, "High-Speed VCSELs for OOK and Multilevel PAM Modulation," presented at *2017 IEEE Optical Interconnects Conference (OI)*, Santa Fe, NM, USA, June 2017.

[K] A. Larsson, J.S. Gustavsson, E. Haglund, E.P. Haglund, **T. Lengyel**, and E. Simpanen, "High-Speed VCSELs for OOK and Multilevel PAM Modulation," presented at *2017 IEEE Photonics Conference (IPC)*, Orlando, FL, USA, Oct. 2017.

[L] Z. S. He, **T. Lengyel**, Y. Jian, H. Zirath and A. Larsson, "Optoelectronics Enabled Dense Patch Antenna Array for Future 5G Cellular Applications," in *Proceedings of the 43rd European Conference on Optical Communications*, Gothenburg, Sweden, Sept. 2017.

[M] J. Chen, Z. S. He, **T. Lengyel**, K. Szczerba, P. Westbergh, J. S. Gustavsson, H. Zirath and A. Larsson, "An Energy Efficient 56 Gbps PAM-4 VCSEL Transmitter Enabled by a 100 Gbps Driver in 0.25 μm InP DHBT Technology," *Journal of Lightwave Technology*, vol. 34, no. 21, pp. 4954−4964, 2016.

[N] J. M. Castro, R. Pimpinella, B. Kose, Y. Huang, B. Lane, K. Szczerba, P. Westbergh, **T. Lengyel**, J. S. Gustavsson, A. Larsson and P. A. Andrekson, "48.7-Gb/s 4-PAM Transmission Over 200 m of High Bandwidth MMF Using an 850-nm VCSEL," *Photonics Technology Letters*, vol. 27, no. 17, pp. 1799−1801, 2015.

[O] J. M. Castro, R. Pimpinella, B. Kose, P. Huang, B. Lane, K. Szczerba, P. Westbergh, **T. Lengyel**, J. S. Gustavsson, A. Larsson and P. A. Andrekson, "Investigation of 60 Gb/s 4-PAM Using an 850 nm VCSEL and Multimode Fiber," *Journal of Lightwave Technology*, vol. 34, no. 16, pp. 3825−3836, 2015.

Acknowledgement

I would like to express my gratitude towards my examiner Prof. Peter Andrekson for giving me the opportunity to join the Photonics Laboratory and supporting me in my quest to better understand fiber optics. This has not only helped me develop a more mature scientific mindset and a professional attitude as a researcher, but it has helped me grow as a person. I want to thank my supervisor Prof. Magnus Karlsson for his patience and dedication in our discussions regarding simple and not so simple matters. Throughout my research I have always received support from Prof. Anders Larsson regarding everything VCSEL related, be it getting to comprehend them better or writing about them. I'd like to express my thanks to Profs. Sheila Galt and Jörgen Bengtsson for their excellent pedagogical skills that have helped improve my way of sharing knowledge with others.

I am forever grateful towards Dr. Krzysztof Szczerba for sharing his knowledge with me, his unwavering generosity and encouraging guidance when I had my doubts. After all these years, we can still continue our conversations as if they never ended.

I thank all my former and current colleagues at the Photonics Laboratory for making my time here such an unparalleled experience, whether it was an interesting discussion about Sweden or types of cinnamon or any other occasions when I required a little help from my friends. Thanks to all the sportsmen from Photonics Laboratory and MC2 for helping me stay energetic and fit! I'd like to thank Jeanette Träff for helping me with all the administrative or organizational issues.

Shout-outs go to Dr. Clemens Krückel: too many fond memories to list, let's just hope we are still Fit for a King; to Dr. Josué Parra Cetina: thanks for showing me that no matter what life throws at you, a positive attitude will help you catch and throw back. Special recognition to Dr. Attila Fülöp, Dr. Erik Haglund and Dr. Lars Lundberg for being excellent conversationalists and partners in after-work fun. Not forgetting my partner in crime, Dr. Emanuel Haglund, in making everyone shake their heads in disbelief after all those pun-

matched plays on words. Ewa Simpanen, thanks for all the VCSELs and for being such an awesome "roomie"!

Finally I'd like to express my deepest gratitude towards my family and friends for all their support regardless of distance. Judit, my love and life, thank you for being so patient and understanding through all these years and for always being there for me. Ervin, my son, your smile and laugh is a light in any darkness.

Tamás Lengyel

Göteborg
April 2019

This work was financially supported by the Knut and Alice Wallenberg Foundation and the Swedish Foundation for Strategic Research.

List of Abbreviations

4-PAM	4-pulse amplitude modulation
AC	alternating current
AOC	active optical cable
AWGN	additive white Gaussian noise
BCH	Bose-Chaudhuri-Hocquenghem
BER	bit error ratio
BPG	bit pattern generator
bps	bits per second
CAP	carrierless amplitude and phase
CMOS	complementary metal-oxide semiconductor
DC	direct current (context dependent)
DC	datacenter (context dependent)
DBR	distributed Bragg reflector
DMD	differential mode delay
DMT	discrete multitone
DSP	digital signal processing
EA	error analyzer
EDFA	erbium-doped fiber amplifier
EMB	effective modal bandwidth
FEC	forward error correction
HPC	high performance computing
IM/DD	intensity modulation with direct detection
ISI	inter-symbol interference
LED	light emitting diode
MCAP	multi-band carrierless amplitude phase modulation
MMF	multi-mode fiber
MPN	mode partition noise
OFL	overfilled launch

OOK	on-off keying
PAM	pulse amplitude modulation
PAPR	peak-to-average power
PIC	photonic integrated circuit
QAM	quadrature amplitude modulation
RF	radio frequency
RIN	relative intensity noise
RS	Reed-Solomon
SER	symbol error ratio
SMF	standard mono-mode fiber
SNR	signal-to-noise ratio
SOI	silicon-on-insulator
SWDM	shortwave wavelength division multiplexing
TIA	transimpedance amplifier
VCSEL	vertical cavity surface emitting laser
VNA	vector network analyzer
VOA	variable optical attenuator

Contents

Chapter 1

Introduction

The term “information superhighway” [1] was coined in the 1980s to reflect the access to Internet telecommunications network hosting the immeasurable information available for anyone using the Internet. This metaphor hides an acute understanding of how information is traveling from host to user through a complex infrastructure spanning the globe. Starting a video stream on any of our devices requires the activation of many network components, but the most important element of the "superhighway" is the optical fiber. When looking at the global fiber network, we can clearly understand the concept of the “superhighway” - the fibers are the roads connecting continents, countries, cities etc. Using multiple cables containing many fibers with multiple wavelengths, we can expand the analogy with lanes of data traffic.

One might think that these highways are only for long-reach applications. However, with the advent of online social media, cloud storage, streaming services, high performance computing we must realize that data exchange must be concentrated in special hubs, usually referred to as datacenters. These buildings host tens of thousands of servers each and the servers are interconnected via very high data rate (above 10 Gbps), short (below 1 km) optical links. Available space, power consumption and cost are major factors in designing such centers, therefore devices in these links must ensure that they minimize these parameters yet they must be mass producible and easily maintained at the same time. Current standards include the parameters for lane rates, wavelengths, packaging, among others.

As with any complex system comprising of high data rate devices (including driver circuitry, receiver electronics, connection interfaces, etc.) industry standards for operation ensure the design, maintenance and quality of these links and provide a basis for research goals. These are discussed in more detail

in Chapter 2. This thesis will present results and techniques related to the new standards including the transition to multilevel modulation formats that are candidates for future standards.

1.1 A short history of fiber optic communication

Throughout history, the means of communicating over large distances effectively was almost exclusively done by transmitting optically detectable symbols or signs. A lighthouse communicates the vicinity of dangerous waters, a painting captures moments of time and imagination through colours and shapes. As a direct communication system, we can consider simple schemes like smoke signals, flag semaphore systems and of course written text interpreted through reading. All rely on optical light reaching our sense of sight.

In 1841 Jean-Daniel Colladon from the University of Geneva, as a way to show students how water flows out of a tank in different jets of water, collected sunlight and illuminated the jets [2]. Through optical refraction he achieved total internal reflection and students could see the various jets lit from the inside while the classroom was in darkness. At the time this effect provided great entertainment value: Colladon's water jets made it into opera productions and a fountain spewing illuminated jets of water was a landmark attraction in the World Fair of London in 1851. In 1842, Jacques Babinet, a specialist in optics also found this phenomena intriguing and also showed that this transmission of light is possible through curved glass rods [3]. These fundamental discoveries spurred the research of improving the manufacture of very thin glass fibers, yet

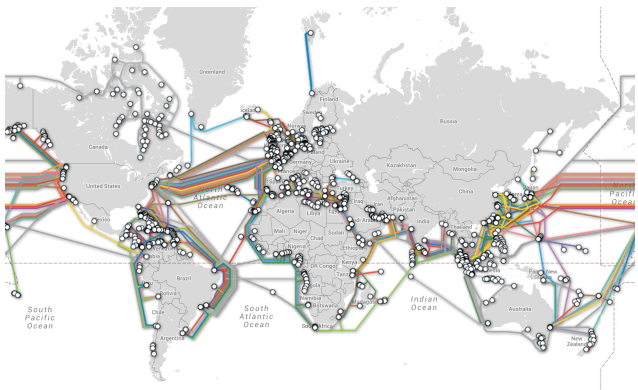

Figure 1.1: The global fiber optic network (www.submarinecablemap.com)

still only for aesthetic pleasure. In 1930, Heinrich Lamm first transmitted an image of a light bulb through a bundle of optical fibers, making this the first instance of transmission of information through optical fiber. Unfortunately, further progress was stalled as image quality was poor and such applications were marginal.

Not only until 1960, when Theodore Maiman presented the world's first working laser [4], did fiber optics receive renewed interest. The transistor was already invented and fiber manufacturing by 1970 showed promise when Corning announced its newest fiber with 20 dB/km attenuation [5] - a milestone achievement, since the 1966 prediction made by Charles K. Kao and George Hockham [6] showed that this is the acceptable limit for fiber optic communications to be successful. Kao also showed that it is glass impurities that cause the bulk of attenuation, therefore research sped up in improving manufacturing processes. In 2009, Kao shared the Nobel Prize in Physics "for groundbreaking achievements concerning the transmission of light in fibers for optical communication" [7].

The parallel progress and research in high-speed electronics, laser design and silica glass manufacturing culminated in a successful field trial in 1978 of a 44.7 Mbps transmission system in Atlanta, USA using 820 nm lasers and fibers with a loss of only 6 dB/km [8]. Fast evolution followed. By 1988 the first transatlantic cable, the TAT-8 link was deployed using 1300 nm transmission wavelength with 280 Mbps throughput [9].

These aforementioned links suffered from major limitations in speed, since the repeaters that helped to overcome signal degradation over the spans could not keep up with the modulation speeds provided by transmitter electronics. Additionally, they were an inefficient design: the optical signal had to be converted to the electronic domain, amplified, then converted back to the optical domain. A new era in fiber optic communication was emerging with the invention of the fully optical erbium-doped fiber amplifier (EDFA) by David Payne of the University of Southampton and Emmanuel Desurvire at Bell Laboratories in 1986 [10] and tailored to the 1540 nm operation wavelength, reported in [11]. This ensured that the transmitted data could increase by hundredfolds and the first ever all-optical transoceanic cable (TAT-12/13) was installed in 1996 in the Atlantic Ocean [12].

Ever since, fiber optic links have encompassed the globe. Fig 1.1 shows the latest map of the intercontinental fiber network. Current technologies are steadily reaching higher and higher throughput with many techniques, such as the use of photonic crystal fibers for improved transmission quality, closely spaced wavelength channels to make use of the low attenuation window of single-mode fibers around 1550 nm, advanced modulation formats making use of all parameters of the light wave, coding and error correction to enhance detection of data symbols, etc.

1.2 Short-reach fiber-optic links

Short-reach communication links (sometimes referred to as datacom links) are almost as old as digital computing. They can either connect computers or provide links within computer components. Even today, a large fraction of links are still copper-based, i.e. the transmission medium is compromised of copper cables. A datacenter is typically a computer or a number of computers that are linked to perform data processing/storage for a specific task. The earliest example of a datacenter was the airline booking system developed by IBM and American Airlines, called the Semi-Automated Business Research Environment, or SABRE [13], launched in the early 1960s. The system was a success and launched the idea of centralized data processing within single large-scale hubs. Many other businesses and companies followed upon this idea, and by 1977 ARCNET was introduced within Chase Manhattan Bank as the first Local Area Network (LAN), connecting up to 255 computers with data rates of 2.5 Mbps [14] using copper cables. For decades, the transmission capabilities of copper was enough for lane rates over short distances. As datacenters evolved, the need for transmission throughput was an ever more demanding challenge for designers who wanted to keep copper cables in their systems. The main physical drawback for these interconnects was the lack of scalability of data rate versus the frequency dependent loss of existing cables: as the required bandwidth is increased, the potential reach of copper decreases. The potential bandwidth available in fiber optics meant that the need to transition to optical interconnects was unavoidable [15].

We have seen which major breakthroughs helped develop the global fiber optic network in the previous section. Similar milestones can be seen in the evolution of short-reach optical connections. The groundbreaking development of the vertical cavity surface emitting laser (VCSEL) in 1979 [16] paved the road for new applications of these revolutionary devices. Among the key benefits of VCSELs compared to their edge emitting counterparts are their low fabrication costs, since reliability, testing and characterization can be simplified. One of the most important features for these lasers is the circular output beam profile, enabling efficient coupling into optical fiber. These advantages have made these lasers the choice for short-reach links found in optical interconnects, consumer electronics, vehicle communication and driver assistance systems [17]. Progress in multi-mode fiber design further propelled the expansion of VCSEL-based interconnects to today's multi-gigabit transmission links. These links are readily available products, packaged into active optical cables, and are implemented according to industry standards, such as FibreChannel [18], Thunderbolt [19], Infiniband [20] and Ethernet [21].

1.3 Thesis outline

This thesis deals with current approaches regarding multilevel modulation in short-range optical links. Chapter 2 summarizes the characteristics of the components and devices used in these VCSEL-based links and will present standards, and form factors that accommodate these links. The third chapter details the modulation formats used in the experiments and the method of generating them and presents the basic measurement techniques which were used. Chapter 4 discusses the current state-of-the-art approaches in research of this field. The fifth chapter proposes future avenues for research within this field and the final chapter gathers the publications which were the basis of this thesis.

Chapter 2

Short-reach fiber-optic links

Annual global datacenter (DC) IP traffic is predicted to reach 20.6. Zettabytes by the end of 2021, averaging at about 1.7 ZB per month (the evolution of the increase is shown in Fig. 2.1; more than 99% of global network traffic will originate or be processed by datacenters, according to the Cisco Global Cloud index [22]. DCs can be categorized into many categories based on their location or services provided: on-premise Enterprise DCs, Cloud DCs (also referred to as Hyperscale or Mega DCs), edge DCs which are close to populated areas (processing and storing mostly real-time data from businesses and devices used by the local populace) and even planned micro-DCs near telephone towers to handle the emerging traffic of the 5G wireless standard.

The interconnectedness of DCs is a key driving factor in developing links that can support data traffic. Interestingly, the large majority (71.5 % projected value) of data produced by DCs stays within theses hubs, including storage, production and authentication. This trend creates a challenge for network designers and researchers working on the physical layer of creating these high-speed links. The connections related to DCs can be categorized into two main types:

- Intra-DC connections: links within the datacenter itself, typically shorter than 2 km, the focus of this thesis.
- Inter-DC connections: links connecting DCs together within premises or farther, with link lengths up to 120 km.

Another area of data processing where short-reach optical links are applied are the so-called High Performance Computing (HPC) applications, more com-

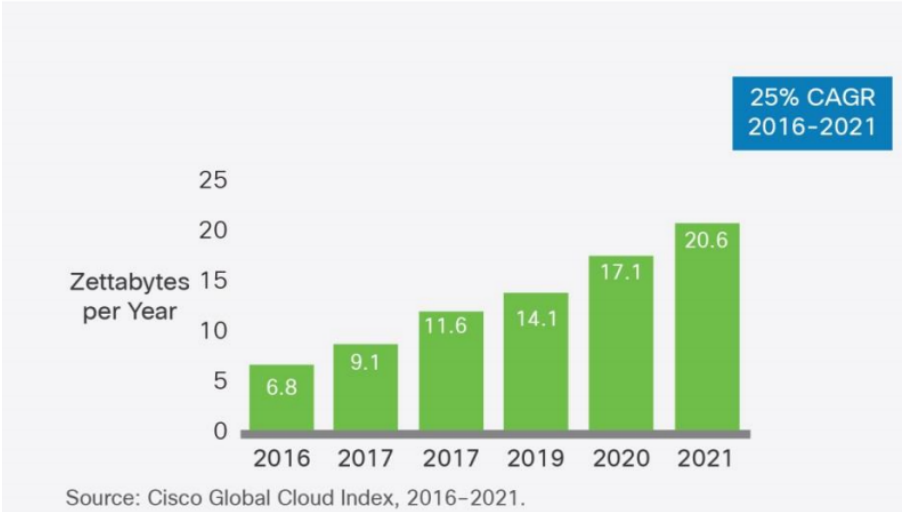

Figure 2.1: Former and predicted global data center IP traffic [22].

monly known as supercomputers. These systems are mainly used for high-end scientific research simulations in weather forecasting, biology, nuclear physics or even cosmology. The first HPC system to use VCSEL-based parallel optics was the Advanced Simulation and Computing (ASC) Purple system installed at the Lawrence Livermore National Laboratory in 2005 [23], reaching a milestone 100 teraFLOPS computing goal. In HPC applications, where data integrity is essential, and bit error ratios (BER) need to be below 10^{-12}, the parallel optical links have to meet extra stringent requirements in terms of reliability, latency (i.e. no digital signal processing in the link) and performance. This means that research into error-free transmission links is always of interest, i.e. solutions that enable the further evolution of HPC. As of the writing of this thesis, the number one system is the Summit system in Oak Ridge National Laboratory, USA [24]. The system uses optical interconnects in its architecture based on the Infiniband standard.

2.1 Intra-datacenter connections

This thesis details research into short-reach optical links, which in the industry are sometimes called datacom links or, in terms of datacenter applications, intra-datacenter connections. As already mentioned in the Introduction, there are many standards by various industry associations which offer solutions to

these needs, namely Ethernet, Infiniband and FibreChannel. The difference between these standards can be shortly described as follows:

- Ethernet[1]: broad scope of applications, but deals mostly with data traffic and form factors of devices.
- Infiniband[2]: as already mentioned, it is a key technology in HPC.
- FibreChannel[3]: a solution focusing on storage are networks (SAN) and information management.

2.1.1 Ethernet

Ethernet is the most well known standard, managed by the Institute of Electrical and Electronics Engineers (IEEE) through the 802 project. Under the 802.3 denomination, the evolution of the standard has seen 10 Mbps copper-based links evolve into the latest standard of links, referred to as 400GbE, accepted in 2017. The evolution of both standards and Ethernet speeds is shown in Fig. 2.2.

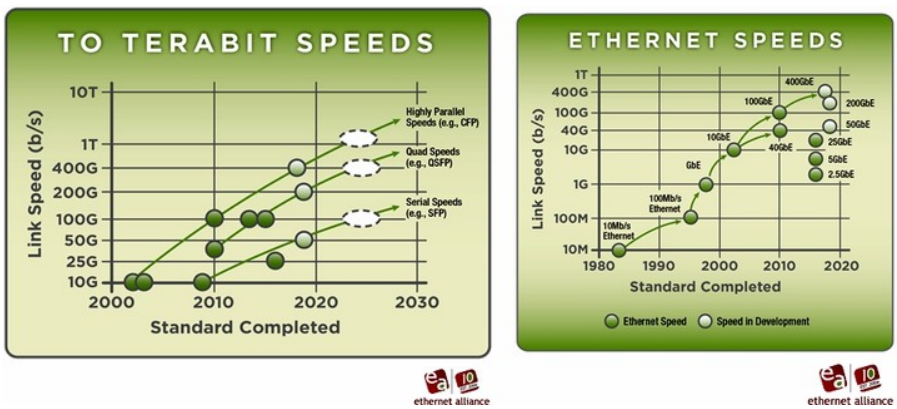

Figure 2.2: The Ethernet Standard road map [21].

2.1.2 Infiniband

Infiniband™, is a collaborative standard between technology drivers who deal with building and selling HPC related devices and low-latency communication links using channel-based, switched fabric interconnect architecture for server

[1] www.ethernetalliance.org
[2] www.infinibandta.org
[3] www.fibrechannel.org

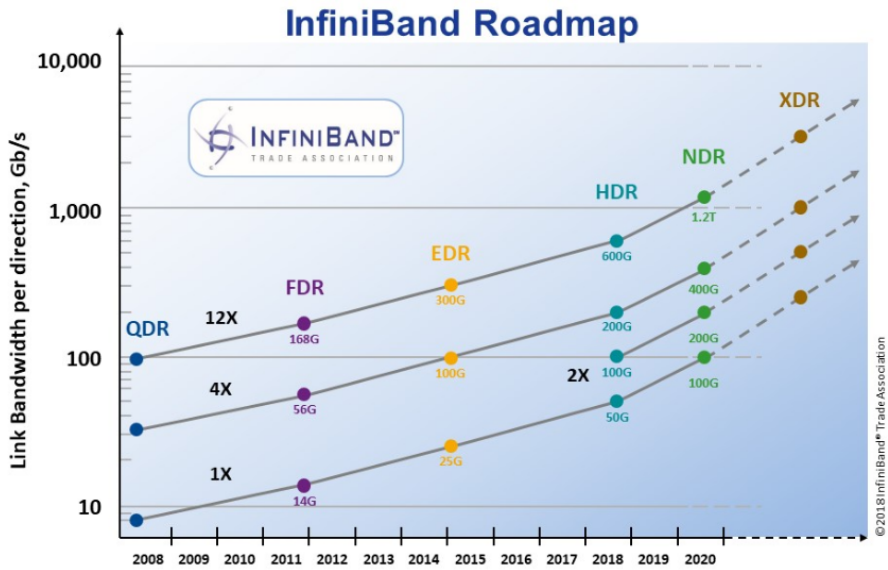

Figure 2.3: The Infiniband™ road map (QDR: Quad Data Rate; FDR: Fourteen Data Rate; EDR: Enhanced Data Rate; HDR: High Data Rate, NDR: Next Data Rate, XDR: eXtended Data Rate) [20].

and storage connectivity. Research laboratories, artificial intelligence developers and national laboratories opt for Infiniband-based architectures when installing HPCs. This means that any research in short-reach optical links encompassing high data rate, low latency solutions (even error-free transmission experiments) are of interest for this standard. As with the other standardized technologies, their latest published roadmap as of this writing (Fig. 2.3) push their goals to ever higher lane rates. The already implemented HDR standard uses the QSFP56 form factor and 850 nm VCSEL-based multimode fiber active optical cabling [25]. Additionally, Infiniband fabric solutions are compatible with Ethernet switches to bolster their application range.

2.1.3 FibreChannel

FibreChannel™(FC) is a high-speed data transfer protocol for computer data storage systems and servers. Its main usage is in storage area networks (SAN), typically using fiber optics as a medium; its main protocol is the Fibre Channel Protocol which runs SCSI commands over its networks. A key characteristic of FC is the provision of in-order and lossless delivery of raw block data. Large

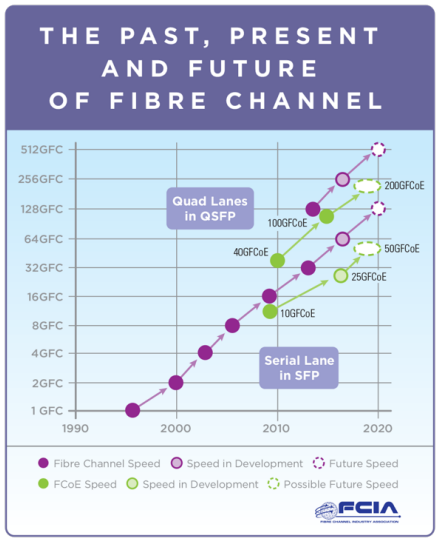

Figure 2.4: The FibreChannel™ road map[18].

FC-based networks rely on their own switched fabric design. Since its inception in 1998, FC has seen doubling in transfer speed every few years since 1996. This is reflected in their historic roadmap and their planned roadmap, see Fig. 2.4. Among the lane rate definitions, the group has also created and developed modules to accommodate the physical layer traffic, e.g. the 128GFC-1TFC module relying on VCSEL transmission and parallel OM4 MMF.

2.2 Inter-datacenter connections

Inter-datacenter interconnects include those between datacenters in metropolitan areas and different cities, with uses as either storage backup or to create a large, but distributed datacenter. To meet latency requirements, these facilities (referred to as Edge DCs) are located up to 120 km apart [26]. These increased distances pose a new challenge to link design, as direct detection schemes can not meet the future 400 Gbps lane rate standard. This is caused by the low tolerance to chromatic dispersion accumulated during transmission, and intensity modulated signals can, in effect, be undetectable without dispersion management. Dispersion compensating fibers (DCF) or Fiber Bragg Gratings (FBG) are go-to options to optically compensate for chromatic

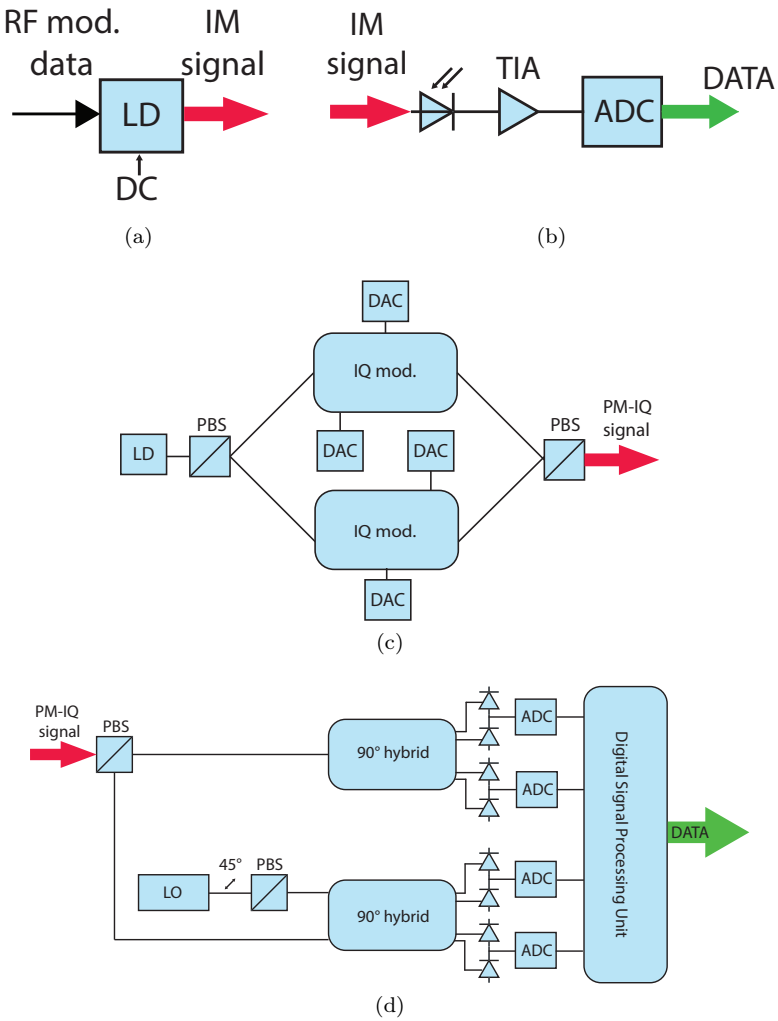

Figure 2.5: Comparison between simplified representations of IM/DD transmitter (a) and IM/DD receiver (b) and coherent, polarization multiplexed transmitter (c) and receiver (d)

dispersion in these links, but may cause latency or additional losses. If left uncompensated, digital signal processing (DSP) might have to be introduced, but can only partially compensate the dispersion [27].

A straightforward solution to the chromatic dispersion found in inter-DC

connections is to use less sensitive modulation formats. There are various approaches that are in consideration. One major alternative is the use of coherent detection [28]. During coherent detection, the receiver performs a linear mapping from the optical field to the electrical signal using the input optical signal from the fiber and a matched local oscillator (LO) laser which serves as an absolute phase reference. The output of the receiver are two currents proportional to the imaginary and real parts of the signal. This enables coding of data into the phase (and amplitude) of the light, and additional digital signal processing can manage the dispersion electronically, track the polarization and compensate for polarization mode dispersion. Of course these additional steps require costly circuitry, at the same time increasing the power consumption. Fig. 2.5 shows a high-level comparison between the transmitter and receiver block diagrams for IM/DD and coherent, polarization multiplexed signal generation. A strong argument for more complex modulation formats is the question of spectral efficiency, namely the efficiency of using the available bandwidth for as many bits of data as possible. Measured in bit/s/Hz, M-PAM formats fall short of coherent modulation formats: one can derive the spectral efficiency of M-PAM as $0.5 \cdot \log_2 M$, whereas polarization multiplexed M^2-QAM offers $4 \log_2 M$ bits/s/Hz efficiency. It is evident from looking at the architectures that IM/DD is a simpler, therefore less costly solution in terms of manufacturing and power efficiency, yet as link lengths increase, considerations regarding coherent transmissions will emerge.

2.3 Form factors for high-speed DC links

The datacenter industry will eventually adopt the 400GbE technology, standardized in IEEE 802.3bs-2017 [29]. As with all standards, the physical layer will have to terminate each link with a transceiver module. Currently there are many competing form factors that try to accommodate the new standard: Octal Small Formfactor Pluggable (OSFP) [30], the latest member on the market; C form-factor pluggable (CFP) and its newest generation, CFP8 [31]; and Quad Small Form Factor Pluggable Double Density (QSFP-DD) [32], the smallest form factor of the three with eight lanes that can achieve up to 50Gbps data rate per lane. Finally, there is a conceptual design called Consortium for On-Board Optics, or COBO [33], planned to be the most power efficient of the four, but is still in development stage. Fig. 2.6 shows the physical form factors: QSFP-DD[1], CFP8[2], OSFP[3] and COBO [3]. Within these solutions it is worth noting that to meet standards, OSFP and QSFP-DD are designed to

[1] `https://bit.ly/2GpseB8`
[2] `https://bit.ly/2UFOZVm`
[3] `https://bit.ly/2D92QfL`
[3] `https://bit.ly/2D92QfL`

incorporate 4-PAM signalling, whereas CFP8 tries to use existing lane rates with a 16x25 Gbps interface and COBO is installed internally to line-card equipment, replacing pluggable interface modules for more direct optical access. Fig 2.7[1] shows the relative sizes of the units and their placement withing a rack environment. It must be noted that the larger the interface, the lower the port density at a cost of worse thermal management.

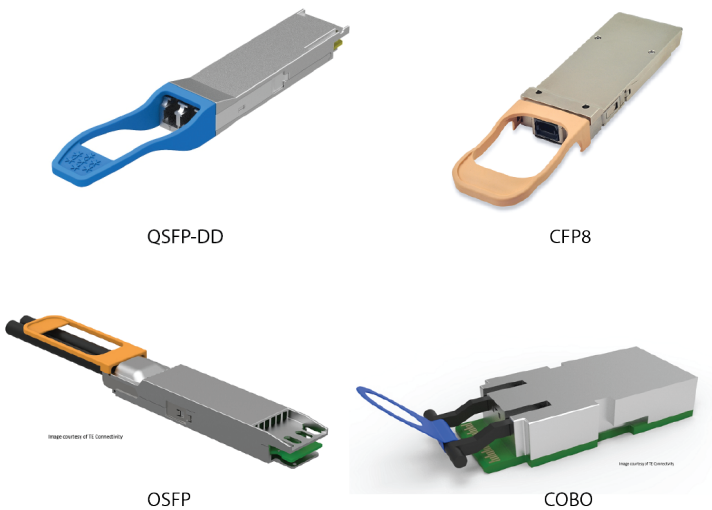

Figure 2.6: Various form factors for 400G applications in DCs: QSFP-DD, CFP8, OSFP and COBO

2.4 VCSEL-based links

The simplest way to describe a communication link is through its basic building blocks. Such a simplified model is shown in Fig. 2.8. The digital data source is the input to the transmitter, which converts the data stream into a format that the channel can propagate over a distance. This can be anything from smoke signals, reflected light from mirrors, sound waves from a speaker, voltage levels or any parameter of a lightwave. The receiver in turn detects this information and converts it back to a digitally interpretable format. In

[1] `https://bit.ly/2WJq7Or`

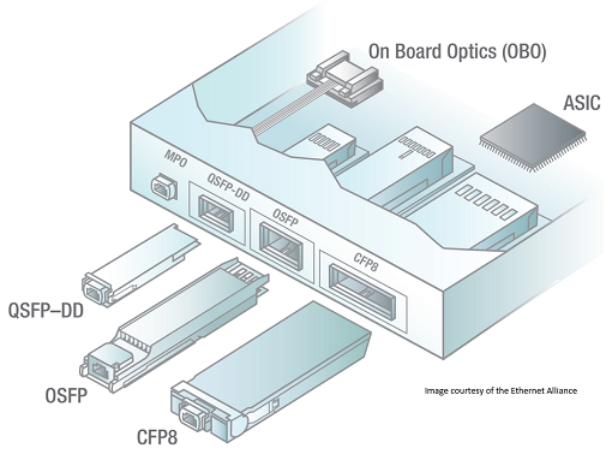

Figure 2.7: Various form factors and their placement within a rack

this thesis, VCSEL-based links are discussed.

To expand the latter into real-world building blocks of a VCSEL-based link, a general setup is shown in Fig. 2.9. It is immediately visible that in this setup the VCSEL –the transmitter– is directly modulated. This approach is critically important, since the use of energy-hungry and bulky external modulators is avoided, increasing overall energy efficiency. The VCSEL is modulated by the electrical signal coming from the digital source, in our case the bit pattern generator which emulates a driver circuit. The laser diode is powered through a bias-T, which combines the high-speed, alternating current (AC)-coupled radio frequency (RF) signal with the direct current (DC) source power. The combined signal is fed to a high-speed RF probe that is in contact with the appropriate electrical pads of the VCSEL. In this scenario the conversion of electrical signals to optical signals is achieved. The emitted beam from the VCSEL facet is coupled into a lens package which first collimates, then focuses the light into a fiber connector tip of the multi-mode fiber

Figure 2.8: Illustration of a simplified digital link.

(MMF). The choice for this fiber type is due to its large tolerance to misalignment, albeit MMFs are more expensive than their single-mode variants. MMFs also relax the spectral requirements on VCSELs, which are therefore generally fabricated as multi-mode devices. This in turn limits the links to intensity modulated/directly detected schemes, where the intensity fluctuations according to the modulation of the VCSEL are detected as information. On the other hand, introducing complexity through more advanced modulation formats will increase costs in the electronics and optoelectronics in such links.

2.5 Datacom light sources

Semiconductor lasers (***L**ight **A**mplification by **S**timulated **E**mission of **R**adiation*) are the fundamental devices in almost all fiber optic links. Both directly and externally modulated lasers have the same principle of operation: they consist of a resonator cavity and a gain region. Photons inside the cavity can create new photon pairs with the same wavelength and phase through recombination of an electron and a hole. The cavity is bound by high reflectivity mirror pairs, confining the photons to perform round trips to further enhance the probability of recombination provided by population inversion in the materials used.

Among lasers there are a few distinct types depending on their cavity design. Fabry-Pérot resonators have a gain region and reflective mirrors, and due to their linear structure, standing waves are generated inside the cavity, therefore they can provide multiple, evenly spaced wavelengths. A more commonly used single frequency laser source is the so-called distributed feedback

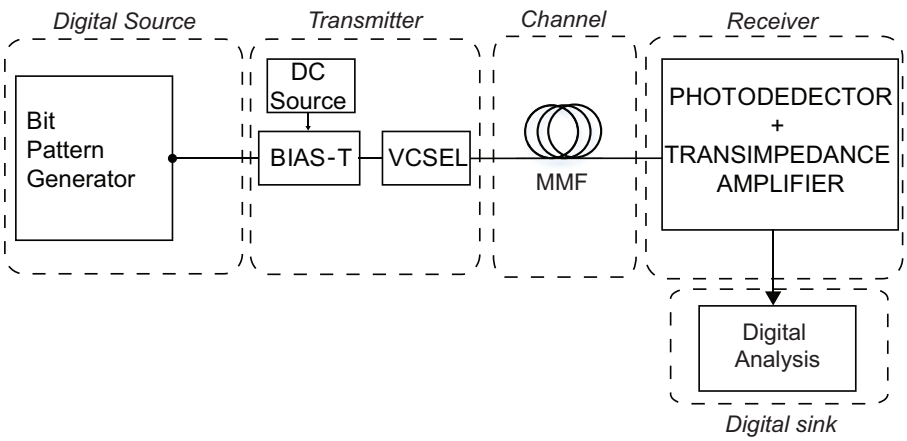

Figure 2.9: Simplified illustration of a VCSEL-based link.

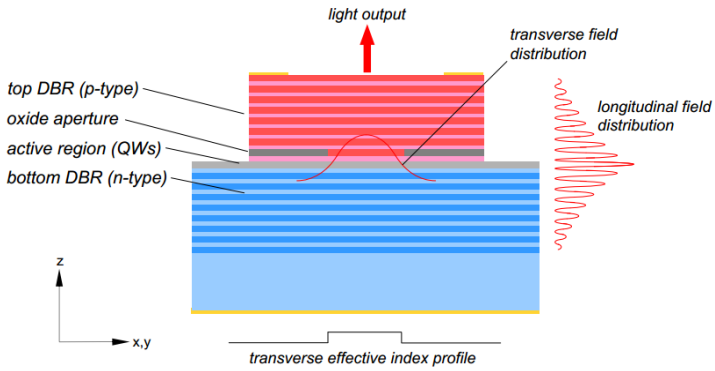

Figure 2.10: Illustration of a simplified VCSEL structure.

laser. Frequency selection is achieved through a diffraction grating etched close to the p-n junction of the laser diode, functioning as an optical filter. This ensures that lasing is performed using this feedback at the selected frequency which helps frequency stability of the device.

As already discussed, VCSELs are the primary light sources for datacom applications. Although light emitting diodes can be considered as a predecessor for VCSELs in short optical links [34], their low modulation bandwidth ultimately meant that they quickly were replaced by lasers in short-reach optical links, but they are still primary devices in visible light communication [35]. The next section will describe VCSELs in more detail.

2.5.1 Vertical cavity surface emitting lasers - VCSELs

VCSELs are constructed by placing a light-emitting semiconductor diode in between crystalline mirror layers with alternating high and low refractive indices. These mirrors are referred to as distributed Bragg reflectors (DBR). This structure enables the light to emit perpendicularly to the layers, providing confinement of light in the longitudinal direction, i.e. vertical to the wafer surface. One must note that there are two distinct field distributions associated with the geometry of a VCSEL. The output spectrum of the VCSEL greatly depends on the aperture diameter, as it controls the transverse modes of the cavity, therefore larger aperture VCSELs have multi-mode behavior. In smaller aperture devices (typically 3 micrometers), the dominant mode is launched from the device and side modes are suppressed. State of the art datacom VCSELs are built with oxide layers near the active region to confine

current into the quantum wells, further increasing the efficiency of conversion. An example of a modern VCSEL structure is shown on Fig. 2.10 [36].

2.5.2 VCSEL characteristics

To understand why VCSELs are the dominant light sources in high-speed optical interconnects, this section will briefly discuss the typical characteristics of these devices, such as the current-power-voltage (IPV), spectrum and small signal modulation response. Temperature dependence of VCSEL characteristics, caused mainly by the change in the refractive index of the DBR layer, will not be detailed in this thesis, as it is outside the scope of the investigations presented.

Output power versus bias current

A primary description for a semiconductor laser is the evolution of its output power as a function of the bias current. A typical IPV curve is shown in Fig. 2.11. Key features on such a curve are the threshold current (I_{th}) and the thermal rollover. The threshold current is the minimum current required for the lasing to start, whereas the thermal rollover indicates the regime where additional biasing does not result in higher output power due to internal heating. The curve shows a linear regime of operation, which is usually chosen as the modulation range, albeit thermal effects are magnitudes slower than typical modulation frequencies. The slope of the linear section is usually described with the slope efficiency: the ratio between the power increase and the bias point shift, measured in ampere/watt. The IPV curve of a VCSEL is temperature dependent – higher device temperature decreases the overall output power and the slope efficiency.

Spectral characteristics

VCSELs are considered as single-longitudinal mode lasers, since their optical cavity is short in the direction of oscillation. Due to the large lateral dimensions, VCSELs support multiple transverse modes. Transverse modes can be suppressed by tailoring the output aperture to a size where only the fundamental mode escapes the device [37]. As aperture size is increased, more light can be coupled from the VCSEL. Therefore, at a given power budget, multi-mode VCSELs offer a better performance, balancing the losses and sensitivity constraints during detection with the cost of chromatic and modal dispersion arising in multi-mode fibers leading to shorter overall reach. Single-mode VCSEL-based links on the other hand suffer less from these distortions,

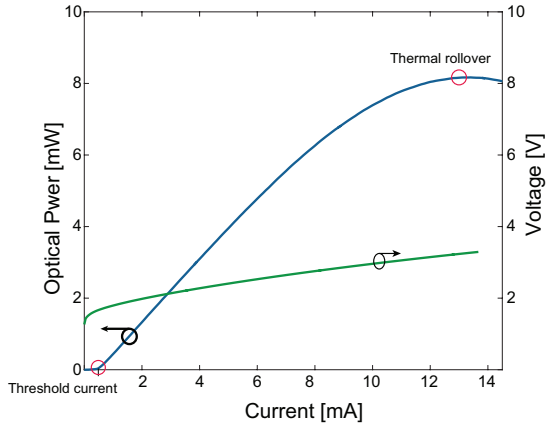

Figure 2.11: Optical output power and diode voltage versus bias current for a VCSEL.

Fig. 2.12 shows typical spectra for both multi-mode (left) and single-mode VCSELs (right) – note the ca. 30 dB suppression of modes of the single-mode device. As the temperature increases, the operating wavelength of the VCSEL shifts to longer wavelengths [38, 39], since the average refractive index of the

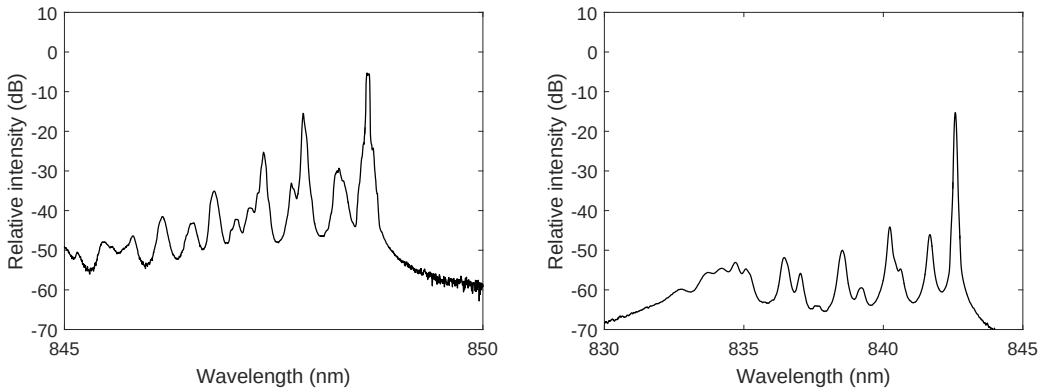

Figure 2.12: Typical output spectrum for multi-mode (a) and single-mode (b) 850 nm VCSEL at 8 mA bias and room temperature. Courtesy of Petter Westbergh.

resonator material changes. A mismatch between the resonance of the DBR mirrors and the gain peak wavelength of the quantum wells (QW) occurs, since the rate of refractive index change is not equal. This ultimately causes lower output power and lower internal quantum efficiency, as there will be carrier leakage from the QWs. With the decrease of internal quantum efficiency, a drop in resonance frequency follows, resulting in the modulation bandwidth to also decrease. Decrease in quantum efficiency also causes the decrease of slope efficiency, i.e. the output power increases at a slower rate when increasing bias current than at lower temperatures.

Small-signal modulation

A key characteristic of a VCSEL is its modulation bandwidth, measured by the S21 response. Typically the –3 dB bandwidth is considered as the modulation bandwidth of the device. From a system point of view, the VCSELs should possess a flat, resonance peak-free frequency response (often termed as "damped") [40] to avoid any overshooting that potentially could introduce inter-symbol interference (ISI) in multilevel modulated links. Of course, this does not change the fact that overall, a VCSEL-based link will behave as a band-limited channel, causing ISI. As the bias point is increased, the resonance frequency increases until thermal saturation effects become dominant. As the temperature of the device is increased, the resonance frequency drops, since the photon density is reduced in the gain region [41].The frequency response of a state-of-the-art VCSEL [42] is shown for various bias currents in Fig. 2.13 [43].

Noise characteristics

As with all semiconductor lasers, VCSELs also possess noise sources. The most widely discussed noise is relative intensity noise (RIN), inherent in all lasers. The source of RIN is spontaneous emission in lasers, which gets coupled into the lasing modes [44]. This results in optical power fluctuations on the useful signal, therefore contributing to signal degradation and power penalty. Usually RIN is measured by subtracting the spectra of the VCSEL turned on at a given bias point and when it is turned off (i.e. thermal receiver noise) and is measured over a finite frequency range, thus its unit is denoted in dB/Hz. The RIN spectrum typically shows a single resonance peak for single and multimode VCSELs [45], but often multiple modes can emerge and show numerous peaks. Above threshold currents, the overall RIN on the measured frequency range quickly decreases, the resonance peak shifts outside of this range and the RIN level reaches the shot noise limit for the detected photocurrent. A

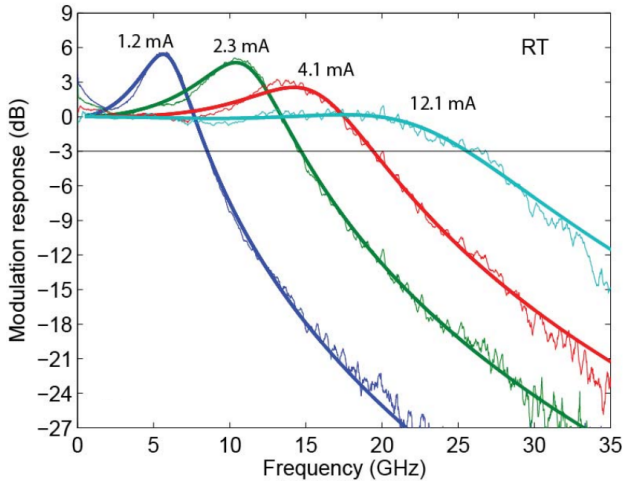

Figure 2.13: Modulation response of a 7 μm VCSEL at various bias points at room temperature.

typical measured RIN spectrum can be seen on Fig. 2.14. As VCSEL designs evolved, modern VCSELs now possess RIN below -140 dB/Hz, further aiding a higher SNR and meeting industry standards [46].

Mode partition noise (MPN) is also a source of signal degradation. It can be caused by the geometry of the coupling to the fiber, where multiple modes compete and during coupling and propagation through multi-mode fiber, these selected modes can effectively add amplitude noise to the transmitted optical signal [47]. MPN directly affects RIN properties, resulting in the aforementioned multiple peaks [45]. Recent studies have calculated and analyzed VCSEL RIN and MPN correlation experimentally [48]. MPN can be reduced by wavefront shaping, significantly improving transmission over MMF links, as experimentally shown in [49].

2.5.3 VCSELs for optical interconnects

As mentioned in Section 1.2, VCSELs for short-reach optical interconnects (OIs) benefit from many attractive attributes, such as low en-masse production costs and low power consumption, among others. The operation wavelengths of today's VCSELs in OIs is still largely 850 nm for the following main reasons: the development of high performance VCSELs showed that the aluminum-gallium-arsenide (AlGaAs) material system showed a balance of high performance and an uncomplicated manufacturing process due to the

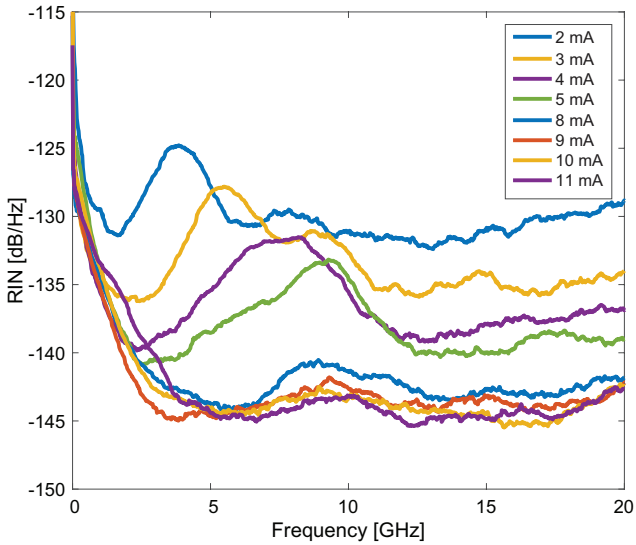

Figure 2.14: Example of RIN spectra for a multi-mode VCSEL at various bias points.

lattice match of the materials [50]. Additionally, MMFs could be easily aligned with high tolerance and coupling efficiency to the circular output beam of the VCSEL, whereas SMFs would suffer from alignment difficulties and poor performance at 850 nm (e.g. becoming multimode fibers themselves, as the cut-off wavelength of SMFs is near 1200 nm).

850 nm VCSEL-based OIs do, however, have their drawbacks, which become more apparent as datacenters grow in size and require ever larger lane rates. This translates into longer OI lengths and, accordingly, poorer performance due to the limitations imposed by MMF characteristics (see. Section 2.6) over such distances. The solution to increase both reach and data rates almost naturally necessitates the shift to higher wavelengths in such links [51]. The following sections will briefly discuss these devices.

850 nm VCSELs

To this day, the most mature manufacturing process for datacom VCSELs belongs to 850 nm devices. As mentioned previously, these devices are based on the GaAs material system and mirrors are fabricated using $Al_xGa_{1-x}As$ compounds. This results in lattice-matched material layers that increase the reliability and lifetime of these devices. Current generations of 850 nm VCSELs employ quantum wells in the active region and oxide-confined apertures to

enhance the radiative recombination rates and to decrease threshold currents through current confinement to the active region, as well as transverse optical confinement. This technique was crucial in the development of energy efficient sub-mA threshold, reliable VCSELs [52].

1060 nm VCSELs

GaAs-based VCSELs technology is still considered superior to indium-phosphide (InP) in terms of speed, energy-efficiency and cost-efficiency [53]. This material system can be extended to operation wavelengths of around 1100 nm without affecting the reliability of the devices [54]. This technology has great potential as a competitor to InP-based externally modulated lasers or VCSELs [55, 56] or silicon photonics solutions [57]. The drive behind 1060 nm VCSEL development is the improved overall performance over standardized MMFs (OM4 and OM5) with respect to fiber attenuation and chromatic dispersion (see Section 2.6). Due to the induced strain in the structure, however, VCSELs at these wavelengths showed overall lower slope efficiency due to higher internal optical loss stemming from the quadratic wavelength dependence on free-carrier absorption [58].

Similarly to its 850 nm counterpart, these longer wavelength VCSELs can be fabricated as single-mode devices. Recent research has shown that utilizing the benefits from the longer wavelength (attenuation below 1 dB/km and chromatic dispersion around –30 ps/nm/km versus typical values of ca. 2 dB/km and ca. –80 ps/nm/km at 850 nm in the same MMF), it is possible to create longer reach links with comparatively large throughput as with 850nm devices, as shown in [59] and **Paper E**.

Long-wavelength VCSELs

From Fig. 2.17 one can see that both attenuation and dispersion values are lower for MMFs. Shifting wavelengths above 1200 nm results in new options for OIs, namely the use of SMFs, whose performance at the 1310 nm and 1550 nm wavelength windows are well known in long-haul transmission schemes. VCSELs in this wavelength range (Long-wavelength VCSELs - LW-VCSELS) require material systems with the suitable bandgap. The materials of choice are typically InP-based compounds. The difficulty with manufacturing such devices lies in the incompatibility with GaAs-AlGaAs mirror materials. To overcome this obstacle of active region–mirror mismatch, wafer-fused VCSELs were developed using buried tunnel junctions (BTJs) [60]. This innovation has made LW-VCSELs an affordable and high-performance alternative to GaAs-based VCSEL solutions, as presented in [61, 62].

When opting for longer wavelengths, datacenter operators will try to enforce SMF-based links, since their use is deemed "future proof" and SMF

manufacturing cost is significantly lower than MMFs. It is important to note that the "cost" of SMF systems, when first installed, in DCs is multiple of the MMF-based solutions, but one has to take into consideration the long-term costs as well: SMFs possess higher available optical bandwidth and once installed, new cabling is seldom needed during expansion of a network, therefore eliminating the cost of deploying a new fiber-optic network. This benefit will on the long run mitigate the initial costs and if wavelength division multiplexing over these wavelengths will emerge, the already installed network will not need replacement. This, with the low optical absorption in silicon makes LW-VCSELs an attractive solution when considering Si-photonics platforms for interconnect technologies [63].

2.6 Optical fibers for optical interconnects

This section will briefly discuss the MMF and its role in short-reach fiber optic links, including its effects on transmission quality. MMFs are a primary choice for VCSEL-based links mainly due to their large core area (either 62.5 μm or 50μm), making alignment tolerances high, resulting in lowered connectorization costs. Single mode fiber (SMF) is cheaper to manufacture, but in the case of datacenter applications, where millions of short links are present, the aforementioned installation costs outweigh the fiber cabling costs as of today [64]. Another motivation to keep multi-mode fiber-based links is the higher cost of single-mode transceiver modules, manufacturers report an average of 1.5 to 4-5 times higher costs depending on the data rate [65]. The main reasons for this are the already mentioned alignment (both position and angle) tolerances of single mode devices and the requirements set on the output laser beam itself to have an efficient coupling into the fiber. Looking ahead, it is perceivable that more and more SMF links will penetrate into future datacenters, but VCSELs with their low fabrication costs and their superiority in low power consumption will dominate as transmitters.

2.6.1 Multi-mode fibers for optical interconnects

Multi-mode fibers derive their name due to their large numerical aperture compared to the wavelengths they are commonly used for. Typical standardized MMFs have a core diameter of 62.5 μm or 50 μm (compared to 9 μm of a SMF) and the most prevalent technology uses 850 nm VCSELs. MMFs behave as a regular dielectric waveguide with a core with a refractive index n_{core} and a cladding with smaller refractive index $n_{cladding}$, where the relative index change is $\Delta = (n_{core} - n_{cladding})/n_{core} \ll 1$, creating a so-called weakly guiding dielectric waveguide. If we approach the propagation from a ray optics point of view, we can assume that beams of light travel by means of total in-

ternal reflection, trapping the light inside the core. This simplified description does not cover how modes are propagating. For this, waveguide theory must be introduced using an electromagnetic wave description. Modes keep their initial parameters, such as polarization and transverse distribution along the fiber core. The number of modes can be calculated using the V parameter [66, Ch. 10]:

$$V = 2\pi \frac{a}{\lambda} \sqrt{n_{core}^2 - n_{cladding}^2}, \tag{2.1}$$

where λ is the wavelength of the propagating light and a is the core diameter. Since a is significantly larger than λ in an MMF, V is large and the number of modes is approximated as

$$N_{modes} \approx \frac{4}{\pi^2} V^2. \tag{2.2}$$

This results in many hundreds of modes whether whether the core is 62.5 μm or 50 μm in diameter. With the presence of many guided transverse electric (TE) modes, their electric field E can be written as their superposition:

$$E(x, y, z) = \sum_{j,k} a_{j,k} u_{j,k}(x, y) \exp(-j\beta_{j,k} z), \tag{2.3}$$

where for mode j, k, $a_{j,k}$ is the mode amplitude, $u_{j,k}$ is the mode distribution and $\beta_{j,k}$ is the propagation constant. This means that each mode has a different propagation constant, causing the group velocity to be also different according to the relation between the two:

$$\frac{1}{\nu_g} = \frac{\partial \beta_{j,k}}{\partial \omega}, \tag{2.4}$$

where ω is the angular frequency. This ultimately converts a differential mode delay, causing the effect of modal dispersion [67]. Some modes can be grouped together, as they possess identical or similar group velocities. In weakly guiding waveguides, the solutions to the wave equation result in linearly polarized ($LP_{j,k}$) modes. These modes belong to the same principal mode group m if the condition

$$m = 2k + j + 1 \tag{2.5}$$

is fulfilled [68]. Modal dispersion limits the bandwidth of multi-mode fibers, causing a decrease in reach and achievable data rate for a given fiber length [69].

MMFs have evolved over many years of development. Before the emergence of VCSELs, MMFs had step-index refractive index profiles to accommodate modulated light from light-emitting diodes (LEDs) with their large core area

[70]. These older generation step-index MMFs are now referred to OM1 and OM2. Later developed standard fibers, such as OM3, OM3+ and OM4 are graded index fibers, where there is a gradient change in refractive index inside the core, minimizing the modal dispersion. The standards for these fibers are described in the ISO/IEC 11801 [71], although the standard ITU-T G.651.1 also defines multi-mode fibers from OM2 and above [72].

The transmission reach of MMFs can be described using the modal bandwidth and the effective modal bandwidth (EMB). Modal bandwidth – or more commonly, the bandwidth-distance product – is expressed in MHz·km, and describes the highest signaling rate for a given distance, whereas EMB is the actual modal bandwidth measured using a reference source and pulse. The distinction is made due to legacy LED-based links using the so-called overfilled launch (OFL; the core is fully illuminated to excite all guided modes with a frequency-swept LED), whereas differential mode delay (DMD) profiles are measured by illuminating the core at different radial points with a short pulse emitted from a SMF to ensure a small spot size for better resolution. The resulting plot shows how pulses are delayed in time at different launch positions. An example DMD profile is shown in Fig. 2.16. Table 2.1 summarizes the various OFL and EMB distance-bandwidth products of standardized MMFs.

The past years have shown a new design emerging, whose designation is now widely used as OM5 or referred to as "wideband" multi-mode fiber and has already been approved by the ISO/IEC 11801 Committee as OM5. Typical EMB for OM5 is 4700 MHz·km at 850 nm and 2470 MHz·km at 953 nm, where the latter value is compensated for by lower chromatic dispersion and therefore the EMB requirement is also lower for similar system performance as shown in Fig. 2.17. It is specially designed for the 850-950 nm wavelength range, so that shortwave wavelength division multiplexing (SWDM) is possible. These fibers have an increased effective modal bandwidth. This technique enables the parallel use of tuned VCSELs to transmit usually at two or four distinct wavelengths (850 nm and 940 nm; 850 nm, 880 nm, 910 nm and 940 nm) for both OOK-NRZ [73] and 4-PAM [74–76], the solution depicted in Fig. 2.15[1]. Some manufacturers, such as Corning [77] and OFS [78] have commercially available designs of this standard, as well as the technological association SWDM Alliance[2].

[1] `hhttps://community.fs.com`
[2] `http://www.swdm.org/`

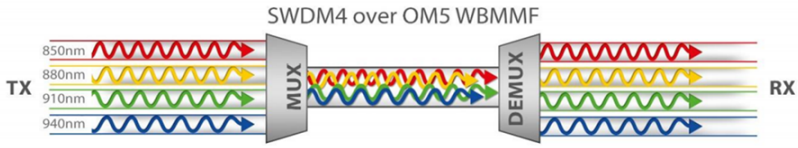

Figure 2.15: A simplified representation of SWDM over OM5 MMF fiber

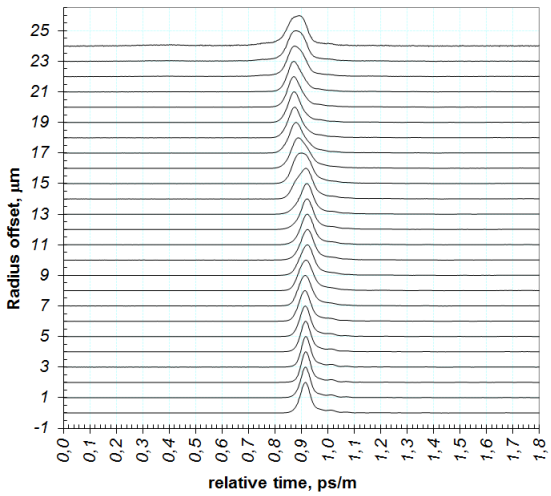

Figure 2.16: Example of the DMD profile of a MMF. Courtesy of J.M. Castro, Panduit Laboratories.

2.6.2 Single-mode fibers for optical interconnects

As we have seen in the previous discussion, MMFs are still currently dominant in the short-reach fiber optic links. New standards further improve their capabilities to accommodate the increasing need for throughput, as discussed when describing OM5 fibers. Additionally, there is research into experimental MMFs optimized for 1060 nm operation wavelength, showcased in [53] and SMFs that have low cut-off frequency (e.g. the prototype fiber used in **Paper E** and [80]) to accommodate single-mode VCSELs operating near the 1060 nm wavelength.

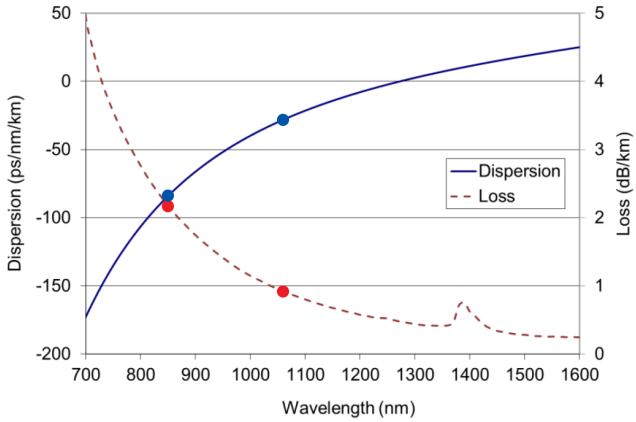

Figure 2.17: MMF chromatic dispersion and attenuation versus wavelength, with operation wavelengths of 850 nm and 1060 nm marked [79].

Table 2.1: OFL and EMB bandwidth-distance product for standardized MMFs

OM Designation	Overfilled launch 850/1300nm [MHz·km]	Effective modal bandwidth 850 nm [MHz·km]	Effective modal bandwidth 953 nm [MHz·km]
OM1 (62.5 μm)	200/500	n.a.	n.a.
OM2 (50 μm)	500/500	n.a.	n.a.
OM3 (50 μm)	1500/500	2000	n.a.
OM4 (50 μm)	3500/500	4700	n.a.
OM5 (50 μm)	3500/500	4700	2470

2.6.3 Multi-core fibers for optical interconnects

Space division multiplexing (SDM) is now a well-established technology in the research of long-haul transmission systems. The key idea is using various techniques to transmit data through multi-core fiber (MCF), a combination of multiple cores within a single cladding or multiple modes in a single core [81]. Although not heavily researched for short-range optical links, SDM may eventually be the next step in solving the increasing demand of throughput in datacenters [82]. It is possible to create VCSEL arrays that are spatially matched to MCFs, as shown in [83], enabling an error-free aggregate data rate of 240 Gbps. Alternately, the light of a single laser source can be used and split, decorrelated and transmitted through the cores, enabling a FEC-enhanced throughput of 700 Gbps [84].

2.7 Optical signal detection and noise

In this discussion we focus on intensity modulation with direct detection (IM/DD) schemes, where the power of the optical signal carries the information. The optical receivers in this case detect the optical signal and convert it to current. This is typically done with simple p-i-n junction photodetectors, whose output current is directly proportional to the incident optical power P_{in}. A photodetector has a given responsivity R_d at a given wavelength and the photocurrent generated is given by:

$$I_{ph} = R_d \cdot P_{in}. \tag{2.6}$$

Signal detection is aided by electric amplifiers after the diode. Most frequently they are current-voltage converting stages, called transimpedance amplifiers (TIA), but seldom voltage amplifiers are used. To convert the detected signal into digitally comprehensible data, decision circuits are needed. These usually include a clock-recovery circuit to synchronize the decision process and the decision circuit compares the output to the specified threshold level at the specified sampling times. In OOK-based transmission two distinct voltage levels are needed and in the case of M-ary amplitude modulation, $M-1$ thresholds form the separation.

A method to describe signal quality is through the signal-to-noise ratio (SNR). It is defined as

$$SNR = \frac{\text{average signal power}}{\text{noise power}} = \frac{\bar{I}_{ph}^2}{\sigma^2}, \tag{2.7}$$

where $\bar{I}$ is the average photocurrent and σ is the root mean square of the noise current. This description is valid in the electrical domain, therefore in this discussion noise sources are all considered electrical. As previously mentioned, the responsivity R_d is the ratio between the output current of the detector and the incident optical power, expressed in Amperes per Watt. This means that the conversion of Watts to Amperes is a square root operation (square law detection).

In this work, three main noise sources are considered after detection:

1. Shot noise
2. Thermal noise
3. RIN

Due to the quantized nature of photons and electrons, the photocurrent fluctuates due to the random electron-hole generation and photon absorption inside the detector, even if the incident optical power is kept constant. This means that the photocurrent will have a small time-varying component: $I(t) =$

$I_{ph} + i_s(t)$, where $i_s(t)$ is assumed to have zero average value. The variance of shot noise is expressed as:

$$\sigma^2_{shot} = 2q(I_{ph} + I_d)\Delta f, \tag{2.8}$$

where q is the elementary charge, I_{ph} is the photocurrent, I_d is the dark current and Δf is the receiver bandwidth [69, Ch.4, Sec. 4.4.1]. Shot noise is directly proportional to the photocurrent, ergo the average optical power.

Thermal noise (i_T) arises from the thermal motion of electrons in resistors, resulting in additional current fluctuations in the total current: $I(t) = I_{ph} + i_s(t) + i_T(t)$. The variance depends on the resistive load's resistance:

$$\sigma^2_T = 4k_B T F_n \Delta f / R_{load}, \tag{2.9}$$

where k_B is the Boltzmann constant, T the temperature, F_N is the noise figure of the amplifier stage after the detector.

RIN originates from the laser source. As already mentioned in 2.5.2, it cannot be considered uniform in distribution because of its resonance peaks, and peaks rising from low frequencies where mode competition is present [85]. At a given (RIN) value, the RIN variance is expressed as

$$\sigma^2_{RIN} = (RIN) I^2_{ph} \Delta f, \tag{2.10}$$

In total we can sum the variances:

$$\sigma^2 = \sigma^2_{shot} + \sigma^2_T = 2q(I_{ph} + I_d)\Delta f + 4k_B T F_n \Delta f / R_{load} + (RIN) I^2_{ph} \Delta f, \tag{2.11}$$

and thus the SNR can be expressed as:

$$SNR = \frac{\bar{I}^2_{ph}}{\sigma^2} = \frac{(R_d \cdot P_{in})^2}{(2q(I_{ph} + I_d) + 4k_B T F_n / R_{load} + (RIN) I^2_{ph})\Delta f}. \tag{2.12}$$

In this thesis, two specific noise limits are referenced. These are:

- Thermal noise limit
- Shot noise limit

A thermal noise limited scenario is when $\sigma_T \gg \sigma_{shot}$. The thermal noise floor is important in defining the receiver sensitivity, and is governed by the bandwidth of the receiver by $4k_B T \Delta f$ and is not dependent on the signal power. If we assume that the power spectral density of thermal noise is constant, thermal noise is mainly driven by the bandwidth. Often receivers are described by their noise-equivalent power (NEP), which is defined as the minimum optical power per unit bandwidth to produce an SNR of 1:

$$NEP = \frac{P_{in}}{\sqrt{\Delta f}}, \tag{2.13}$$

A link can be considered shot noise limited if $\sigma_{shot} \gg \sigma_T$. This can be achieved when the incident optical power is high enough to overcome the thermal noise limit, therefore SNR can not be improved by a higher optical power.

RIN can dominate link noise after detection as it is proportional to the square of the detector photocurrent, i.e. the higher the average received optical power, the higher the RIN induced noise. Therefore it is critical to select low-RIN devices where high detected optical powers are present.

2.8 Power efficiency of VCSEL-based links

So far, the characteristics of VCSELs has been discussed. To create a link, it is of course not enough to have a light emitting device. As depicted in Fig. 2.8, there are many components in a transmission connection. When examining OIs, most focus is spent on the driver and receiver circuitry, as the power consumption for these parts is the highest in any high-speed VCSEL link. The vast majority of the drivers developed rely on complementary metal–oxide–semiconductor (CMOS) technology, a design method that uses a combination of p-type and n-type metal–oxide–semiconductor field-effect transistor (MOSFETs) to implement logic gates and other digital circuits. Some research groups opt for silicon-germanium (SiGe) drivers [86], but they prove more power hungry and costly compared to CMOS [87].

A distinction must be made. Research focusing on driver and receiver circuitry usually report link power efficiency, i.e. the total power of the link divided by the achieved data rate. With regards to VCSELs and their design, there are two metrics found in the literature: the energy-to-data ratio (EDR) which is the voltage across the VCSEL multiplied by the bias current and divided by the achieved data rate ($V \cdot I/BR$) and the dissipated heat-to-data ratio (HDR), which takes the output power produced by the VCSEL into account: $((V \cdot I - P_{opt})/BR)$. Since this thesis deals with links, power efficiency will refer to link power efficiency in the rest of the thesis. State-of-the-art common-cathode designs show energy efficiencies between 0.84 and 3.9 pJ/bit [88–92] and 4.7 pJ/bit for a FinFET CMOS driver with three-tap pre-emphasis in the transmitter and 1-tap DFE and TIA in the receiver [93]. Interestingly, in the same study the design of laser diode drivers has been analytically investigated based on 130 nm SiGe BiCMOS fabrication, and at 45 and 30 Gbps, 1.8 and 1.17 pJ/bit were shown, respectively.

Chapter 3

Pulse amplitude modulation in short-reach VCSEL-based fiber-optic links

In high-speed short-reach optical interconnects MMF-based, intensity modulated, direct detection (IM/DD) schemes dominate current links. The use of this technology is mainly driven by its low implementation cost and simplicity. Costs are determined by the mass production and testing of devices (mainly VCSELs) and complexity of the driver circuitry and detection circuitry, the high alignment tolerance of VCSEL-based MMF links, and the volume used up by interconnects. As datacenters can host hundreds of thousands of interconnects each, another equally important factor when discussing interconnects is the power efficiency, usually expressed in pJ/bit. This usually includes all circuits, the VCSEL, detector and the data processing units, if present.

From the Shannon-Hartley theorem, we can assess the upper bound on the channel capacity in bits per second for an arbitrarily low error rate, assuming the channel noise is additive white Gaussian (AWGN) [94]:

$$C = B \log_2(1 + \frac{S}{N}), \tag{3.1}$$

where C denotes the capacity, B is the channel bandwidth, S is the average received signal power, N is the average power of the noise and interference over the bandwidth. The ratio of the latter two is the signal-to-noise ratio (SNR), described in Chapter 2. It is immediately apparent that increasing available bandwidth will increase the capacity linearly compared to the logarithmic increment by improving the SNR. Since MMFs can behave as a low-pass filter [95], therefore the strongest limitation in interconnects is the available channel bandwidth. In bandwidth-limited, low-pass filtered scenarios, inter-symbol

interference (ISI) rises, meaning that adjacent or subsequent symbols interfere with each other. This can be understood by the following description of an AWGN channel model:

$$y(t) = x(t) * h_c(t) + \nu(t), \tag{3.2}$$

where $x(t)$ is the transmitted signal, $h_c(t)$ is the impulse response of the channel and $\nu(t)$ is AWGN with power spectral density $N_0/2$. In our case, $h_c(t)$ is considered to be the impulse response of a low-pass filter, governed by the channel bandwidth. Low-pass filtering broadens the signal in time, therefore adjacent symbols suffer from artifacts from neighboring symbols. For a sequence of symbols y_k, the sampled received signal values can be expressed as [96, Ch. 9.2]

$$y_k = x_k + \sum_{\substack{n=1 \\ n \neq k}}^{\infty} x_n h_{k-n} + \nu_k, \tag{3.3}$$

where x_k denotes the deisred transmitted symbols, x_n are the transmitted symbols, h denotes the impulse response of the channel and ν_k is the additive noise variable. The desired term, i.e. the transmitted information symbol is symbolized by x_k. The second term represents ISI in the k-th sampling instant.

3.1 Pulse amplitude modulation

For IM/DD systems, such as short-range optical interconnects, amplitude modulation is the most trivial modulation format. Information bits or symbols are assigned to light intensity levels launched by the VCSELs, therefore the constellation diagrams of OOK, the 3-PAM modulation used in **Paper F** and 4-PAM are one dimensional. Since there is a non-negativity constraint in such schemes, the constellation diagrams all have points in the positive domain of the axis, as shown in Fig 3.1.

By increasing the number of modulation levels, the overall spectral efficiency increases. For M-PAM formats, at a fixed bit rate, the bandwidth of the M-ary amplitude modulation is $1/\log_2(M)$ compared to OOK [97].

A powerful qualitative tool to represent data sequences in time is by using eye diagrams. These plots overlay all sampled symbols, and many conclusions can be assessed by analyzing the eye diagrams. A simulated eye diagram for an OOK NRZ signal with and without ISI is shown in Fig. 3.2a and Fig. 3.2b. When looking at eye diagrams, ISI introduces two penalties: power penalties close the eye diagram vertically and timing penalty closes the eye horizontally.

The power penalty for OOK-NRZ systems has been analyzed in [98]. The worst-case ISI power penalty in dB is defined as

$$P_{ISI} = 10\log_{10}\left(\frac{1}{1-E_m}\right), \tag{3.4}$$

where $E_m$is the worst-case eye closure. For OOK the approximation of E_m is

$$E_{m,OOK} = 1.425\exp\left(-1.28\left(\frac{T}{T_C}\right)^2\right), \tag{3.5}$$

where T denotes the symbol period and T_C is the 10%–90% system rise-time. This approximation is valid under a Gaussian channel response and a rectangular input pulse [99]. Extending this to M-PAM, modeling it as three M-1 OOK eye diagrams, using the same system rise time and symbol rate, the eye closure of M-PAM will be:

$$E_{m,M-PAM} = \frac{M}{2}\exp\left(-1.28\left(\frac{T}{T_C}\right)^2\right). \tag{3.6}$$

3.2 Bit error ratio calculation

When discussing high data rate links, BER versus required received optical power is a key metric to assess link performance. BER is defined as the ratio between the number of errors over the total number of bits received:

$$BER = \frac{N_{error}}{N_{bits}}, \tag{3.7}$$

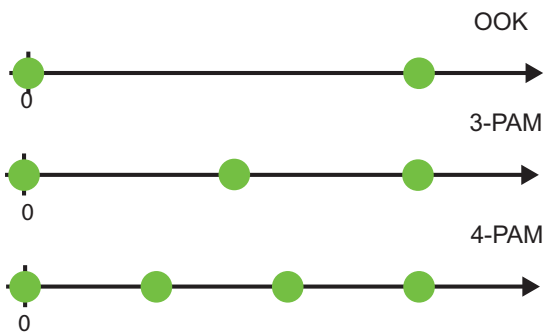

Figure 3.1: Constellation diagrams for OOK and 4-PAM

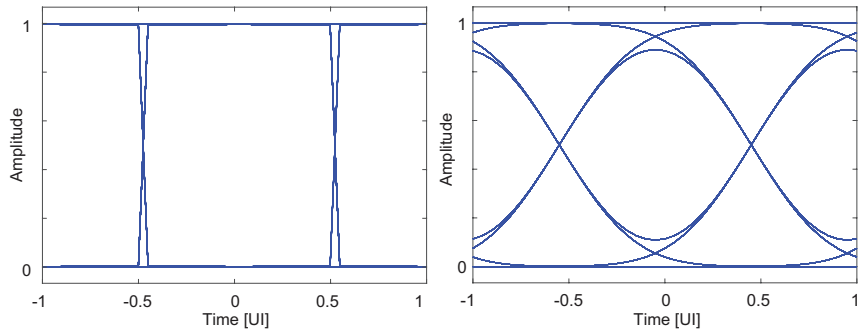

Figure 3.2: Simulated eye diagrams for OOK-NRZ with no ISI (a) and with ISI (b)

When conducting experiments, it is useful to compare the measured values versus theoretically calculated values in order to understand sources of impairments, such as implementation penalties or previously discussed limitations. For different modulation formats, BER can be calculated from the symbol error ratio (SER) by calculating the bit errors for all combinations of errors possible in a symbol, i.e. aggregating the error probabilities of certain transitions. The SER for M-ary amplitude modulation has been derived in [100]. With sufficiently high SNR and Gaussian noise, the SER can be approximated as

$$SER = \frac{(M-1)}{M} \operatorname{erfc}\left(\frac{I_{avg}}{(M-1)\sigma\sqrt{2}}\right), \tag{3.8}$$

where I_{avg} denotes the average photodetector current, σ is the RMS current noise for all symbols and erfc is the complementary error function. Since in this thesis non-negative constellations are used throughout the experiments, as seen in 3.1, we can write the amplitude levels A_i as:

$$A_i = \Delta i, i = 0, 1...M-1, \tag{3.9}$$

where Δ represents a unit amplitude. From here the mean values of the photodetector current and signal power E_s as a function of M can be expressed as:

$$I_{avg} = E[X] = (1/M)\sum_{i=0}^{M} A_i = \frac{\Delta(M-1)}{2}, \tag{3.10}$$

$$E_s = E[X^2] = (1/M)\sum_{i=0}^{M} A_i^2 = \frac{\Delta^2(2M-1)(M-1)}{6}, \tag{3.11}$$

and from the above, I_{avg}^2 becomes

$$I_{avg}^2 = \frac{3E_s(M-1)}{2(2M-1)}, \tag{3.12}$$

Finally, expressing the SER for any value of M (M=0,1,2...), the SER as a function of M, the signal energy E_s and the power spectral density ($\sigma = \sqrt{N_0/2}$) becomes

$$SER = \frac{(M-1)}{M}\,\mathrm{erfc}\left(\sqrt{\frac{3E_s}{2(2M-1)(M-1)N_0}}\right), \tag{3.13}$$

simulated and analyzed in **Paper F**. The BER of a modulation is dependent on its labeling of symbols, i.e. how bits are assigned to a symbol. The Hamming distance is the number of positions where a string of bits is different, denoted as d. In the scope of this thesis, we distinguish between natural labeling and Gray-labeling of symbols [101]. For Gray-mapping $d = 1$, however, other variants of coded modulation may result in other bit-to-symbol mappings. Gray mapping, if, applied facilitates error correction. Compared to OOK and assuming AWGN in the link, the optical power penalty for M-PAM at the same symbol rate has been calculated in [102] as

$$P_{pensym} = 10\log_{10}(M-1), \tag{3.14}$$

which, in the case of 4-PAM translates into 4.8 dB, since 4-PAM requires three times the modulation amplitude of a NRZ waveform at the same symbol rate to achieve the same BER. Similarly, when comparing M-level PAM compared to OOK at the same bit rate, we calculate the optical power penalty as

$$P_{penbit} = 10\log_{10}\left(\frac{M-1}{\sqrt{\log_2(M)}}\right). \tag{3.15}$$

This indicates that for 4-PAM, 3.3 dB more power is required compared to OOK for the same BER at a given data rate. It is clear that although the bandwidth requirement for 4-PAM is halved compared to OOK, more optical power is needed to achieve the same BER. This indicates a trade-off between power efficiency (i.e. the overall power required to generate a high-SNR 4-PAM signal) and bandwidth efficiency.

To generate OOK or 4-PAM signals in laboratory circumstances, one can achieve this in two ways: either use a high bandwidth Bit Pattern Generator (BPG) to create a stream of binary rectangular pulses or use a programmable arbitrary waveform generator (AWG), which can be programmed to store and create custom pulses. Using a BPG has the advantage of enabling real-time

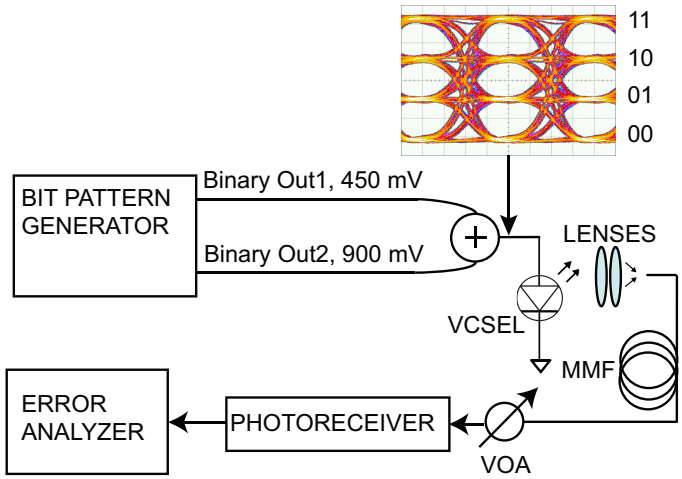

Figure 3.3: Generation of naturally labeled 4-PAM signals using a BPG and two decorrelated binary signals with the generated electrical 4-PAM signal in the inset.

analysis and BER measurement, since an error analyzer (ER) can be synchronized with the BPG. On the other hand, mathematically optimized pulses with the AWG gives the freedom to utilize various form of pre-emphasis or pulse shaping, as presented in [103]. This approach however typically requires offline processing of sampled data and leads to digital signal processing (DSP) in installed links, ultimately increasing power consumption. In the work presented in this thesis, generation of signals was done by using a BPG. Fig. 3.3 shows the method of creating naturally labeled 4-PAM signals.

The BPG transmits two PRBS bit streams, with a given delay offset (usually half of the sequence length to obtain all transitions and acceptable BER measurements) on two branches. For 4-PAM, the amplitude difference has to be a factor of two, so that all levels are equally spaced. A high-bandwidth coupler combines the two branches to form the driving signal to the VCSEL. This electrical signal (seen in the inset) is carried to the externally biased VCSEL via a bias-T to a high-speed probe matching the distance between the signal-ground-signal pads (referred to as the pitch of the probe). The modulated VCSEL optical output is coupled into a MMF fiber by a lens package. After this stage, additional fiber can be inserted. The fiber is then connected to a variable optical attenuator (VOA) so that the received optical power can be changed before detection with a photoreceiver that includes a linear transimpedance amplifier. The converted signal then can be displayed on an

oscilloscope or analyzed with the EA. The EA can not distinguish between all three thresholds of the 4-PAM signal, therefore it has to be treated as three stacked OOK signals. The three level error thresholds, (LERs, denoted as LER_1, LER_2 and LER_3) will produce three BER curves, and assuming that errors are occurring between neighboring decision levels in the low-BER regime, the total BER in the case of natural labeling can be given by

$$BER_{total} = \frac{1}{2}LER_1 + LER_2 + \frac{1}{2}LER_3. \tag{3.16}$$

In this section fundamental modulation considerations were presented. As with all digital links, challenges arise when pushing towards ever higher data rates and transmission lengths. The next section will address the techniques used in state-of-the-art research. When discussing these topics, it must be noted that "error-free" transmission means that the BER is below 10^{-12} with a specified confidence level. Confidence levels are introduced as a means to eliminate uncertainties arising from measurements too short to give a clear metric of BER or avoid measurements which are unnecessarily long. A standard industry confidence level (CL) for BER measurements is 95% [104], where CL is defined as

$$CL = 1 - \exp(-N_{bits} \cdot BER), \tag{3.17}$$

which when rearranged gives the number of bits, N_{bits} required for a given BER and confidence level:

$$N_{bits} = \frac{-\ln(1 - CL)}{BER}. \tag{3.18}$$

In this thesis, all measurements were performed in agreement with the above methodology regarding the confidence level and minimum number of errors.

3.3 Extending the reach of VCSEL-based fiber optic links

Pre-emphasis

As seen from the Shannon capacity calculation, the available bandwidth linearly increases the throughput of the channel. A method to enhance link bandwidth, and consequently decrease ISI, is by manipulating the pulse shapes at the transmitter so that high frequency components are amplified at the cost of the lower frequency components, i.e. transferring energy to higher frequencies. This method of pulse shaping is called pre-emphasis. Implementing the technique on the transmitter side is frequently done by feed-forward equalization (FFE), using finite impulse response (FIR) filters with a series of tap weights to adjust the frequency response beyond the channel's own response. FFEs

are filters whose branches delay the input signal. The output $y[k]$ of a FIR filter with input $x[k]$ is:

$$y[k] = \sum_{n=0}^{N} b_n x[k-n] \tag{3.19}$$

where N is the order of the filter and b_i are the coefficients. The simplified frequency response of such a filter can be denoted as

$$H_{2\pi}(\omega) = \sum_{n=\infty}^{\infty} h[n] \cdot (e^{i\omega})^{-n} = \sum_{n=0}^{N} b_n (e^{i\omega})^{-n} \tag{3.20}$$

The time domain representation of the simplest two-tap FFE filter that has been used in **Paper A** and **Paper E** can be described as

$$y(t) = x(t) + c_1 x(t - \Delta t) \tag{3.21}$$

or, in terms of frequency

$$y(t) = e^{j\omega t} + c_1 e^{j\omega(t-\Delta t)} \tag{3.22}$$

Within the scope of this thesis, filter optimization was performed for values of the delay (the fraction of a symbol period, Δt) and coefficients c_n. This results in a symbol-spaced FIR filter, whose transfer function becomes

$$H(f) = \sum_{n=0}^{N-1} c_n e^{j\omega\Delta t} \tag{3.23}$$

where c_1 was considered to be a negative value, i.e. inversed data.

The main advantage of this method is that it requires relatively low power if implemented with an active circuit or can be passively realized, as shown in **Paper B** and **Paper C**. Fig. 3.4 shows pre-emphasis schematically, using time-domain signal representation. Fig. 3.5 shows the block diagram of FFE. In **Paper A** and **Paper E** a two-tap pre-emphasis was achieved with discrete components for OOK; optimal points were calculated and implemented experimentally.

Equalization techniques

There are numerous types of equalization techniques after detection. They can broadly be categorized into two types: adaptive and fixed equalizers. The key difference between the two is the way they are implemented: fixed equalizers

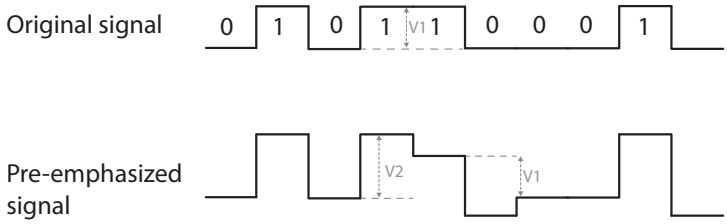

Figure 3.4: Explanatory diagram of pre-emphasis and de-emphasis using time-domain waveforms.

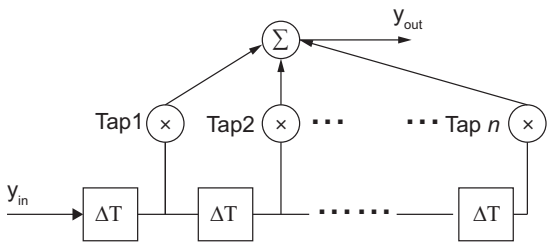

Figure 3.5: Example of how FFE pre-emphasis is generated using FIR filters.

have set values as tap coefficients and adaptive equalizers measure the channel and have a feedback loop to update coefficients.

The adaptive equalization discussed within the scope of the thesis is the least mean squares equalizer (LMSE). This algorithm updates equalizer taps per received symbol, referred to as symbol-spaced equalization. The algorithm is based on the steepest descent method, where after a set of training bits, the equalizer updates the initial filter taps to minimize the difference between the desired symbols and the input signal. Such an equalizer was implemented and used in **Paper C**. Its method of updating follows the recursive equations below:

$$\begin{aligned} e(n) &= d(n) - \mathbf{w}^H(n)\mathbf{u}(n) \\ \mathbf{w}(n+1) &= \mathbf{w}(n) + \mu\mathbf{u}(n)e^*(n) \end{aligned} \tag{3.24}$$

where $e(n)$ is the estimation error based on the training sequence, $d(n)$ is the desired signal, $\mathbf{w}$ are the filter coefficients, $\mathbf{u}$ is the input signal vector and μ is the step-size for the algorithm. A drawback of the LMS is that it may diverge if the step size is not chosen carefully.

Forward error correction

Forward error correction (FEC) is a powerful tool for controlling errors over a noisy channel. The general idea of FEC is to code the data with redundancy without having to resend the data again. This requires special algorithms both to code and decode the data. The first modern error correcting code is attributed to Richard Hamming in 1950, labeled as the Hamming(7,4) code [105].

The advantage of using FEC is the reduction in requirements on BER and received optical power in short-range links at the expense of increased complexity from coding-decoding. This complexity introduces overhead in the data, therefore the effective data rate decreases. Additionally, FEC can potentially add unwanted latency in these links (arising from the processing of the data stream), therefore codes with low error-correcting capabilities are a preferred choice. The codes are conventionally labeled (n, k, t), where n is the code length, k is the number of information bits and t is the number of correctable bits. The code rate thus is k/n and the overheads (the error correcting part of the data) are therefore calculated by the ratio $(n/k) - 1$. These block codes, later generalized by Bose-Chaudhuri-Hocquenghem and referred to as BCH codes correct random bit errors. Unfortunately, for low BERs, the t=1 Hamming codes are insufficient and the more computationally heavy BCH codes are needed. An example for Hamming-code (t=1) based FEC BER requirements were investigated in **Paper B**. FEC has been present and introduced in optical interconnects in the Infiniband standard [106] and Ethernet 100GBASE-SR4 standard [107]. These standards use the Reed-Solomon (RS) error correction codes, also present in optical storage devices, such as DVDs and Blu-Ray discs. RS codes are powerful in correcting burst (or symbol) errors, therefore when the BER is low, RS is a viable solution.

Chapter 4

State-of-the-art and trends in short-reach optical Interconnects

We have established basic approaches to extend the capabilities of VCSEL-based short-reach optical links. Among these are pulse shaping, pre-emphasis, post-equalization, FEC and combinations thereof. Fig. 4.1 visualizes the achieved transmission distances and data rates for such links taken from [108–128]. There are numerous link and modulation designs competing for the future implementations of optical interconnects. A brief description of these will follow in this chapter.

4.1 Modulation

4.1.1 Pulse amplitude modulation

It is clear that there is great competition between various modulation formats and DSP techniques accompanying the data transmission. As discussed before, costs of building a datacenter with VCSEL-based optical links is heavily cost driven, i.e. the lower the price per gigabit of data, the more likely the technology will be implemented. The so-called legacy systems, which are based IM/DD using 850 nm VCSELs and MMF are still dominating current systems, but there are many new avenues where optical interconnects can evolve. The new generation of wideband MMFs (the soon-to-be OM5 standard) gives rise to possibilities to use longer wavelength VCSELs, i.e. 980 nm and above. The motivation behind these new wavelengths is the overall better performance in MMF fibers: chromatic dispersion and attenuation are lower at these wavelengths with existing OM4 fibers, therefore increase in reach is

directly possible. It is undecided which longer wavelength VCSEL-based interconnects will replace or co-exist with the 850 nm standard: the desire for at least 40 Gbps OOK has been achieved with 980 nm VCSELs, as shown in [129, 130], including 4-PAM modulation [131]. 1060 nm VCSELs are also emerging as a potential candidate – transmission over 1 km of MMF at 25.78 Gbps OOK was demonstrated in [59], 40 Gbps was reported back-to-back in [132] and 50 Gbps over 1 km of low cut-off SMF in **Paper E** and 50 Gbps 4-PAM in [133].

There is also a high possibility that within a few years, 1550 nm VCSELs and SMF-based links will emerge, as discussed in Chapter 2.6.2. Required reach within datacenters will increase and an all-SMF infrastructure will enable a more cost-effective network, e.g. due to the scalability of SMF throughput with wavelength division multiplexing (instead of parallel MMFs) or the one-time installation of the SMF fiber network. As shown in Fig. 4.1 the longest reach points were all possible with 1550 nm devices [110, 114, 115, 121].

4.1.2 Discrete multi-tone transmission (DMT)

DMT is a baseband multi-carrier modulation, where multiple orthogonal sub-carriers are used to divide link bandwidth into many narrow bands with data transmission in each band [134]. Most frequently quadrature amplitude modulation (QAM) is used for each sub-carrier. The orthogonal sub-carriers are generated with inverse Fourier transform and on the receiver side, and reversed independently during demodulation from each sub-carrier. The advantage of such a scheme is its flexibility in allocating the number of bits and power for each sub-carrier depending on the SNR. This technique for allocation is sometimes referenced as bit loading. A disadvantage of DMT (similarly to orthogonal frequency division multiplexing) is its high peak-to-average power ratio (PAPR). The more sub-carriers are used, the higher PAPR is, ultimately decreasing power efficiency of the transmission. Additionally, computation-heavy DSP is needed for synchronization and the Fourier-transformations involved. In the context of interconnects, the increased complexity of the scheme also contributes to higher power consumption.

Recent research has shown that pre-distortion with DMT modulation can create VCSEL-based links with throughputs of up to 144 Gbps [135], although relying on hard-decision FEC with 7% overhead. This, of course, as with any FEC scheme increases the power consumption ins short links, as has been shown in [136].

4.1.3 Multi-band carrierless amplitude phase modulation (MCAP)

CAP modulation is a multidimensional and multilevel modulation scheme, first proposed in 1970 [137]. CAP, as its name implies, does not use carriers, instead, filters with orthogonal waveforms are used to separate data streams. Multidimensional CAP has been suggested for short-reach optical links using VCSELs with varying complexity [138, 139]. Multi-band CAP [140] divides the CAP signal into smaller sub-bands tailored to the SNR, and adjusts the QAM baud rate accordingly. As with all complex transmission schemes, the circuitry required to create the modulation potentially increases the overall cost of implementation, although its flexibility in adapting to data traffic can compensate for this [141].

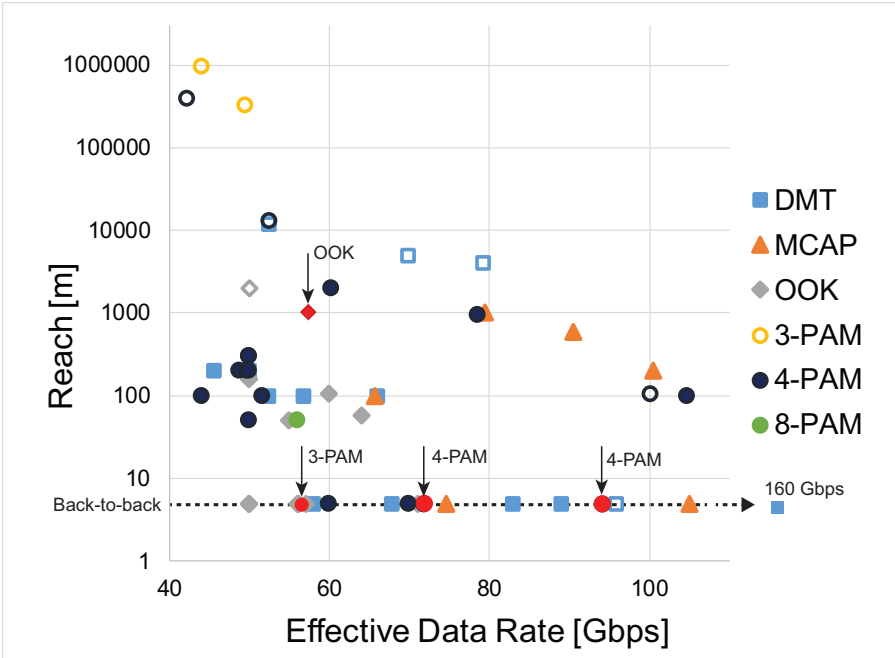

Figure 4.1: Examples of VCSEL-based links above 50 Gbps. Data rates presented are without FEC overhead. Red shapes with arrows show results in this work. Hollow markers show experiments using VCSELs and SMF with wavelengths between 1530 and 1550 nm.

4.2 Coherent detection

Coherent detection for inter-DC connections was briefly discussed in 2.2, where an example polarization-multiplexed coherent transmission scheme was presented. As this thesis covers VCSEL-based links, it is worth to explore the possibilities within these types of links for coherent detection. The output of a VCSEL indeed possesses orthogonal polarization states, but due to their material structure, the polarization stability of VCSELs discussed so far is difficult to control. There have been of course attempts at just coherent detection schemes using VCSELs [142] and have been successful in passive optical networks as laser sources and local oscillators [143]. All these efforts are still ultimately unpopular in academic circles, as the complexity and power consumption of such solutions is much larger than existing IM/DD solutions due to the added circuitry and digital signal processing. On the other hand, increased link length will eventually lead to the need to solve the issue of chromatic dispersion over these distances.

4.3 Power consumption and power efficiency

When looking at DCs or HPC applications, it is evident that millions of point-to-point links can be present. This of course poses the question: how much power should be designated to such an enterprise? There are few data on how much a hyperscale DC actually consumes, but the reported values range in the tens of megaWatts [144]. A datacenter is of course a complex architecture, and there are many power-hungry devices involved in not only the storage, but the processing of data. It is important to note that of all the power required to keep a DC running, only around 5% of energy is required to power the communications systems inside [145]. Although this is just a fraction of the total required energy, any advance in cutting down power consumption is beneficial for any datacenter operator and user.

Within the research of short-reach optical interconnects, much attention is focused on the overall power consumption of the link. In most cases, this rests on the active optical cable (AOC) and the form factor supporting it, detailed in Section 2.3.

4.4 Short wavelength division multiplexing

As mentioned in Chapter 2, SWDM is a way to implement a simple wavelength division multiplexing with VCSELs and the aforementioned wideband MMF fiber with the use of multiplexers with wavelength selective mirrors and similarly constructed demultimplexers. This approach, using the same concept

that is used in the Coarse Wavelength Division Multiplexing (CWDM) standards used in the longwave 1310 nm region operating over single mode fiber, has shown that with four wavelengths between 850 nm–940 nm, 400 Gbps net data rate can be achieved with a single OM5 fiber [146], paving the way to terabit links if SWDM is extended to more wavelengths. This technology is supported by the SWDM Alliance, which includes both fiber manufacturers and datacenter providers.

4.5 Photonics integration

The desire to have integrated photonic devices drives research in silicon photonics. The goal of this technology is to reduce the conversions between the electric domain and the optical domain based on a silicon platform, i.e. integrate the laser source, modulator and accompanying devices on a single chip. Optical interconnects can greatly benefit from the evolving silicon photonics technology, as integration can reduce the footprint and power consumption, in turn increase density of devices without traditional discrete optics [147].

Further steps within photonic integration go beyond interconnects. Optical elements will replace existing electrical components at the board and module level, by integration of optical waveguides. Silicon-on-insulator (SOI) and silicon-nitride (SiN) are two major integration platforms which are CMOS compatible, commonly referred to as silicon photonics. Silicon photonics is the most promising technology to create photonic integrated circuits (PICs), such as waveguides and optoelectronic transceiver modules on a silicon chip. Such integration allows very dense and power efficient single-chip, multi-purpose PICs, with low cost and low power consumption. Unfortunately, silicon does not provide efficient lasing conditions due to its bandgap structure. A challenge therefor is to integrate efficient light sources, such as VCSELs to these PICs. There have been many successful demonstrations of VCSELs integrated to such chips. A hybrid solution of heterogeneously integrated 850 nm VCSEL on silicon a chip with data rates reaching 20 Gbps has been reported in [148, 149], and 1310 nm VCSEL on SOI [150]. Further experiments using distributed feedback lasers show great potential at data rates beyond 100 Gbps using SMF [151].

The compatibility with CMOS allows photonics integration can pave the way to the spectrally more efficient coherent detection schemes. There have been successful realizations of such solutions in the past few years such as the one found in [152], and the platform has shown capabilities to be an attractive solution in the 400GbE standard [153].

Chapter 5

Conclusions and future outlook

Optical interconnects have shown great technological steps forward and have driven the research into many areas of fiber optics, optoelectronics and electronics. The ever increasing demand for data, computing power and storage ensures that this technology will evolve as more datacenters are built.

The research in this thesis has shown a few aspects of where optical interconnects can evolve. There is still great potential in existing 850 nm VCSEL-based links, as shown in Paper **??**, where the possibilities of transitioning from OOK to 3-PAM or 4-PAM is discussed, the latter with regards to VCSEL design. This trend to migrate to multilevel modulation formats is evident from the latest research papers on short-range optical links presented in the References. This is further aided by test and measurement vendors who are developing instruments for testing of 4-PAM signals, eliminating the issues of breaking up the multilevel signal into subsignals. It is therefore interesting to pursue the understanding of 4-PAM and its many new features, such as lower tolerance to laser nonlinear dynamics, RIN, etc.

Applying pre-emphasis and pulse shaping to 4-PAM signals is a powerful technique to overcome link bandwidth. This thesis has presented pre-emphasis with discrete components for OOK in **Paper A** and 4-PAM in **Paper B**. Further detailed analysis of pre-emphasis is needed for 4-PAM links, with a VCSEL equivalent circuit model to accommodate for modulation level-based VCSEL dynamics.

Error-free operation is of course desirable in any link, but is not always achievable. This thesis has incorporated the use of simple FEC in **Paper B** and **Paper C**, relaxing the requirements of operation. Designing links with low overhead FEC keeps net data rates high, latency low enough to be considered for high performance computing.

As discussed in the closing section in Chapter 3, moving operation wavelengths of VCSELs near or above 1000 nm introduces further benefits in terms of performance using MMFs. With the introduction of OM5 fibers and fibers specially designed for this window, 4-PAM with its lower bandwidth requirement than OOK has potential in this new area, so research in the future should also be focused on 1060 nm VCSEL-based 4-PAM links with increased emphasis on power-efficiency.

All these approaches can be combined, and be the foundation for future, high-speed multilevel modulated optical interconnects.

Chapter 6

Summary of papers

Paper A

"Sensitivity Improvements in an 850 nm VCSEL-based Link using a Two-tap Pre-emphasis Electronic Filter," *Journal of Lightwave Technology*, vol. 45, no. 9, pp. 1633-1639, May 2017.

This paper presents two-tap pre-emphasis of OOK driving signals to increase link bandwidth and benchmarks performance to signaling without pre-emphasis. Two different approaches are simulated, optimized and experimentally verified compared to signaling without pre-emphasis. First, equal amplitude pre-emphasis is investigated (the amplitudes of the pre-emphasizing signal and non-pre-emphasized signals are equal), with a 9% increase in achievable error-free data rate back-to-back. The second approach keeps the eye openings equal, i.e. the modulation amplitudes are equal. This scheme increased the achievable error-free data rate by 27% at 0 dBm sensitivity back-to-back.

My contribution: I performed the simulation and optimization of tap values for the pre-emphasis schemes with KS. I built the experimental setup and performed all measurements and analysis and wrote the paper. Results were also presented at the *41st European Conference on Optical Communications*, Sept. 2015 (Valencia, Spain).

Paper B

"Demonstration of a 71.8 Gbps 4-PAM 850 nm VCSEL-based Link with a Pre-emphasizing Passive Filter," in Proceedings of the *42nd European Conference on Optical Communications*, Sept. 2016, paper Th.2.P2.SC4.6

This paper presents a passively pre-emphasized real-time 4-PAM optical link. A net data rate of 71.8 Gbps is achieved supported by a Hamming-code based FEC scheme and requiring no post-processing.

My contribution: I built the experimental setup, performed all measurements and data analysis and wrote the paper. Results were also presented at the *42nd European Conference on Optical Communications*, Sept. 2017 (Düsseldorf, Germany)

Paper C

"94-Gb/s 4-PAM Using an 850-nm VCSEL, Pre-Emphasis, and Receiver Equalization," *Photonics Technology Letters*, vol. 28, no. 22, Nov. 2016.

This paper presents a passively pre-emphasized 4-PAM optical link with 94 Gbps net data rate. Receiver equalization was realized offline using a least-mean-square equalizer.

My contribution: I assisted in the measurements and wrote the code for the equalizer. I co-authored the paper.

Paper D

"Impact of Damping on 50 Gbps 4-PAM Modulation of 25G Class VCSELs," *Journal of Lightwave Technology*, vol. 35, no. 19, pp. 4203-4209, 2017.

In this paper the effects of interrelated slope efficiency, RIN, and damping of 850 nm oxide-confined 25G class VCSELs on 50 Gbps 4-PAM signal generation have been investigated. The measured characteristics and transmission measurements conclude that with moderately damped VCSELs, best overall performance (including error-free operation back-to-back) for 4-PAM modulation is achieved.

My contribution: The VCSELs were fabricated by PW. Simulation of RIN-dependent power penalties were made by KS. I performed the measurements, data analysis and wrote the paper.

Paper E

"Pre-emphasis enabled 50 Gbit/s transmission over 1000 m SMF using a 1060 nm single-mode VCSEL," *Electronics Letters*, vol. 54 , no. 20 , pp. 1186 - 1187, 2018.)

In this paper, a pre-emphasis enabled 1000 m long single-mode 1060 nm VCSEL–SMF link operating error-free at 50 Gbps with no digital signal processing or forward error correction required was presented. To achieve this, a low cut-off prototype SMF with negative dispersion and the large effective area was used.

My contribution: The VCSELs were fabricated by ES. The experimental fibers were provided by Corning Inc.. I built the experimental setup, performed all measurements and data analysis and wrote the paper.

Paper F

"Investigation of 3-PAM transmission in a 850 nm VCSEL-based link," *submitted to Optics Express*

In this paper, a 3-PAM modulated transmission in a VCSEL-MMF link was investigated. Theoretical comparisons were made with OOK and 4-PAM. Transmission experiments showed that 3-PAM outperforms both OOK and 4-PAM in a bandwidth limited link with 100 m of MMF.

My contribution: The VCSELs were fabricated by Petter Westbergh. The theoretical background was provided by MK and EA. I created the simulations and built the experimental setup, performed all measurements and data analysis and wrote the paper.

Bibliography

[1] W. D. Marbach, "The Dazzle of Lasers," *Newsweek*, no. January 3, 1983.

[2] D. Colladon, "On the reflections of a ray of light inside a parabolic liquid stream," *Comptes Rendus*, vol. 15, pp. 800–802, 1842.

[3] J. Babinet, "Note on the transmission of light by sinuous canals," *Comptes Rendus*, vol. 15, p. 802, 1842.

[4] T. H. Maiman, "Optical and Microwave-Optical Experiments in Ruby," *Phys. Rev. Lett.*, vol. 4, no. 11, pp. 564–566, 1960.

[5] F. P. Kapron, D. B. Keck, and R. D. Maurer, "Radiation losses in optical waveguides," *Appl. Phys. Lett.*, vol. 17, no. 10, pp. 423–425, 1970.

[6] K. C. Kao and G. A. Hockham, "Dielectric-fibre surface waveguides for optical frequencies," *Electr. Eng. Proc. Inst.*, vol. 113, no. 7, pp. 1151–1158, 1966.

[7] "The Nobel Prize in Physics 2009." `http://www.nobelprize.org/nobel_prizes/physics/laureates/2009/`.

[8] I. Jacobs, "Atlanta Fiber System Experiment: Overview," *Bell Syst. Tech. J.*, vol. 57, no. 6, pp. 1717–1721, 1978.

[9] "History of the Atlantic Cable & Submarine Telegraphy - Cable Signalling Speed." `http://atlantic-cable.com/Cables/speed.htm`.

[10] S. Poole, D. Payne, and M. Fermann, "Fabrication of low-loss optical fibres containing rare-earth ions," *Electron. Lett.*, vol. 21, no. 17, pp. 737–738, 1985.

[11] R. Mears, L. Reekie, I. Jauncey, and D. Payne, "Low-noise erbium-doped fibre amplifier operating at 1.54μm," *Electron. Lett.*, vol. 23, no. 19, p. 1026, 1987.

[12] P. Trischitta, M. Colas, M. Green, G. Wuzniak, and J. Arena, "The TAT-12/13 Cable Network," *IEEE Commun. Mag.*, vol. 34, no. 2, pp. 24–28, 1996.

[13] R. Head, "Getting Sabre off the ground," *IEEE Ann. Hist. Comput.*, vol. 24, no. 4, pp. 32–39, 2002.

[14] M. Stott, "Two Decades of Networking," *ARCNETworks*, 1998.

[15] A. Alduino and M. Paniccia, "Interconnects: Wiring electronics with light," *Nat. Photonics*, vol. 1, no. 3, pp. 153–155, 2007.

[16] H. Soda, K.-i. Iga, C. Kitahara, and Y. Suematsu, "GaInAsP/InP Surface Emitting Injection Lasers," *Jpn. J. Appl. Phys.*, vol. 18, no. 12, p. 2329, 1979.

[17] O. Strobel, R. Rejeb, and J. Lubkoll, "Communication in automotive systems: Principles, limits and new trends for vehicles, airplanes and vessels," in *2010 12th Int. Conf. Transparent Opt. Networks*, pp. 1–6, 2010.

[18] "Fibre Channel Industry Association." `http://fibrechannel.org/`.

[19] "Thunderbol™Technology: Technology Brief." `https://www.intel.com/content/www/us/en/architecture-and-technology/thunderbolt/thunderbolt-technology-brief.html`.

[20] "InfiniBand® Trade Association." `http://www.infinibandta.org/`.

[21] "IEEE P802.3ba 40Gb/s and 100Gb/s Ethernet Task Force." `http://www.ieee802.org/3/ba/`.

[22] "Cisco Global Cloud Index: Forecast and Methodology, 2016–2021 White Paper - Cisco." `https://www.cisco.com/c/en/us/solutions/collateral/service-provider/global-cloud-index-gci/white-paper-c11-738085.pdf`.

[23] "IBM ASC Purple." `https://asc.llnl.gov/computing_resources/purple/`.

[24] "Summit â€“ Oak Ridge Leadership Computing Facility." `https://www.olcf.ornl.gov/olcf-resources/compute-systems/summit/`.

[25] Mellanox Technologies, "200GbE QSFP56 MMF Transceiver," tech. rep., 2018.

[26] R. Nagarajan, M. Filer, Y. Fu, M. Kato, T. Rope, and J. Stewart, "Silicon Photonics-Based 100 Gbit/s, PAM4, DWDM Data Center Interconnects," *J. Opt. Commun. Netw.*, vol. 10, no. 7, p. B25, 2018.

[27] O. Agazzi, M. Hueda, H. Carrer, and D. Crivelli, "Maximum-likelihood sequence estimation in dispersive optical channels," *J. Light. Technol.*, vol. 23, no. 2, pp. 749–763, 2005.

[28] E. Ip, A. P. T. Lau, D. J. F. Barros, and J. M. Kahn, "Coherent detection in optical fiber systems," *Opt. Express*, vol. 16, no. 2, p. 753, 2008.

[29] "802.3bs-2017 - IEEE Standard for Ethernet - Amendment 10: Media Access Control Parameters, Physical Layers, and Management Parameters for 200 Gb/s and 400 Gb/s Operation," tech. rep., 2017.

[30] "Octal Small Form Factor Pluggable." `https://osfpmsa.org/index.html`.

[31] "CFP Multi-Source Agreement." `http://www.cfp-msa.org/`.

[32] "Quad Small Form Factor Pluggable Double Density MSA." `http://www.qsfp-dd.com/`.

[33] "Consortium for On-Board Optics (COBO)." `https://onboardoptics.org/`.

[34] D. H. Hartman, "Digital high speed interconnects : a study of the optical alternative," *Opt. Eng.*, vol. 25, no. 10, pp. 1086 –1102, 1986.

[35] Y. Pei, S. Zhu, H. Yang, L. Zhao, X. Yi, J. Junxi Wang, and J. Li, "LED Modulation Characteristics in a Visible-Light Communication System," *Opt. Photonics J.*, vol. 3, no. 02, pp. 139–142, 2013.

[36] A. Larsson, *Semiconductor Optoelectronics: Device Physics and Technologies*. Chalmers University of Technology, 2013.

[37] M. Grabherr, M. Miller, R. Jaeger, D. Wiedenmann, and R. King, "Commercial VCSELs reach 0.1-W CW output power," *Proc. SPIE 5364, Vertical-Cavity Surface-Emitting Lasers VIII*, vol. 5364, pp. 174–182, 2004.

[38] J. Perchoux, A. Rissons, and J.-C. Mollier, "Multimode VCSEL model for wide frequency-range RIN simulation," *Opt. Commun.*, vol. 281, no. 1, pp. 162–169, 2008.

[39] R. Michalzik and K. J. Ebeling, "Operating Principles of VCSELs," in *Vertical-Cavity Surface-Emitting Laser Devices* (H. Li and K. Iga, eds.), pp. 53–92, Springer, 2003.

[40] E. P. Haglund, P. Westbergh, J. S. Gustavsson, and A. Larsson, "Impact of damping on high-speed large signal VCSEL dynamics," *J. Light. Technol.*, vol. 33, no. 4, pp. 795–801, 2015.

[41] R. Safaisini, J. R. Joseph, D. Louderback, X. Jin, A. N. Al-Omari, and K. L. Lear, "Temperature Dependence of 980-nm Oxide-Confined VCSEL Dynamics," *IEEE Photonics Technol. Lett.*, vol. 20, no. 14, pp. 1273–1275, 2008.

[42] P. Westbergh, E. P. Haglund, E. Haglund, R. Safaisini, J. S. Gustavsson, and A. Larsson, "High-speed 850 nm VCSELs operating error free up to 57 Gbit/s," *Electron. Lett.*, vol. 49, no. 16, pp. 1021–1023, 2013.

[43] P. Westbergh, R. Safaisini, E. Haglund, J. S. Gustavsson, A. Larsson, M. Geen, R. Lawrence, and A. Joel, "High-Speed Oxide Confined 850-nm VCSELs Operating Error-Free at 40 Gb/s up to 85°C," *IEEE Photon. Technol. Lett.*, vol. 25, no. 8, pp. 768–771, 2013.

[44] K. K. Petermann, *Laser Diode Modulation and Noise*. Kluwer Academic Publishers, 1991.

[45] L. G. Zei, S. Ebers, J. R. Kropp, and K. Petermann, "Noise performance of multimode VCSELs," *J. Light. Technol.*, vol. 19, no. 6, pp. 884–892, 2001.

[46] H. Li, P. Wolf, J. A. Lott, and D. Bimberg, "Relative intensity noise of temperature-stable, energy-efficient 980 nm VCSELs," *AIP Adv.*, vol. 7, no. 2, 2017.

[47] S. K. Pavan, J. Lavrencik, and S. E. Ralph, "New Model for Mode Partition Noise in VCSEL-MMF Links Based on Langevin-Driven Spatio-Temporal Rate Equations," *J. Light. Technol.*, vol. 34, no. 16, pp. 3733–3751, 2016.

[48] J. Lavrencik, S. K. Pavan, V. A. Thomas, and S. E. Ralph, "Noise in VCSEL Based Links: Direct Measurement of VCSEL Transverse Mode Correlations and Implications for MPN and RIN," *J. Light. Technol.*, vol. 35, no. 4, pp. 698–705, 2016.

[49] C. Liang, W. Zhang, L. Ge, and Z. He, "Mode partition noise mitigation for VCSEL-MMF links by using wavefront shaping technique," *Opt. Express*, vol. 26, no. 22, 2018.

[50] K. Iga, "Surface-Emitting Laser-Its Birth and Generation of New Optoelectronics Field," *IEEE J. Sel. Top. Quantum Electron.*, vol. 6, no. 6, pp. 1201–1215, 2000.

[51] Y. Sun, "Recent advances for high speed short reach optical interconnects for Datacom links," in *2017 IEEE CPMT Symp. Japan*, pp. 63–65, IEEE, nov 2017.

[52] M. Feng, C.-H. Wu, and N. Holonyak, "Oxide-Confined VCSELs for High-Speed Optical Interconnects," *IEEE J. Quantum Electron.*, vol. 54, no. 3, pp. 1–15, 2018.

[53] A. Larsson, E. Simpanen, J. Gustavsson, E. Haglund, E. Haglund, T. Lengyel, P. Andrekson, W. Sorin, S. Mathai, M. Tan, and S. Bickham, "1060 nm VCSELs for long-reach optical interconnects," *Opt. Fiber Technol.*, vol. 44, pp. 36–42, 2018.

[54] H. Hatakeyama, T. Anan, T. Akagawa, K. Fukatsu, N. Suzuki, K. Tokutome, and M. Tsuji, "Highly Reliable High-Speed 1.1-μm-Range VCSELs With InGaAs/GaAsP-MQWs," *IEEE J. Quantum Electron.*, vol. 46, no. 6, pp. 890–897, 2010.

[55] O. Ozolins, X. Pang, M. I. Olmedo, A. Kakkar, A. Udalcovs, S. Gaiarin, J. R. Navarro, K. M. Engenhardt, T. Asyngier, R. Schatz, J. Li, F. Nordwall, U. Westergren, D. Zibar, S. Popov, and G. Jacobsen, "100 GHz Externally Modulated Laser for Optical Interconnects," *J. Light. Technol.*, vol. 35, no. 6, pp. 1174–1179, 2017.

[56] S. Spiga, W. Soenen, A. Andrejew, D. M. Schoke, X. Yin, J. Bauwelinck, G. Boehm, and M.-C. Amann, "Single-Mode High-Speed 1.5-μm VCSELs," *J. Light. Technol.*, vol. 35, no. 4, pp. 727–733, 2017.

[57] J. Van Campenhout and Y. Ban and P. De Heyn and A. Srinivasan and J. De Coster and S. Lardenois and B. Snyder and S. Balakrishnan and G. Lepage and N. Golshani and S. Janssen and A. Lesniewska and K. Croes and A. Miller and P. Verheyen and M. Pantouvaki a, "Silicon Photonics for 56G NRZ Optical Interconnects," in *2018 Opt. Fiber Commun. Conf. Expo.*, 2018.

[58] R. W. M. Balkanski, "Semiconductor Physics and Applications," ch. 10.3.1, Oxford: Oxford University Press, 2000.

[59] K. Nagashima, T. Kise, Y. Ishikawa, and H. Nasu, "A Record 1-km MMF NRZ 25.78-Gb/s Error-Free Link Using a 1060-nm DIC VCSEL," *IEEE Photonics Technol. Lett.*, vol. 28, no. 4, pp. 418–420, 2016.

[60] M. Ortsiefer, W. Hofmann, J. Rosskopf, and M.-C. Amann, *Long-Wavelength VCSELs with Buried Tunnel Junction*, pp. 321–351. Berlin, Heidelberg: Springer Berlin Heidelberg, 2013.

[61] F. Karinou, N. Stojanovic, A. Daly, C. Neumeyr, and M. Ortsiefer, "1.55-μm Long-Wavelength VCSEL-Based Optical Interconnects for Short-Reach Networks," *J. Light. Technol.*, vol. 34, no. 12, pp. 2897–2904, 2016.

[62] D. M. Kuchta, T. N. Huynh, F. E. Doany, L. Schares, C. W. Baks, C. Neumeyr, A. Daly, B. Kogel, J. Rosskopf, and M. Ortsiefer, "Error-Free 56 Gb/s NRZ Modulation of a 1530-nm VCSEL Link," *J. Light. Technol.*, vol. 34, no. 14, pp. 3275–3282, 2016.

[63] E. Kapon and A. Sirbu, "Long-wavelength VCSELs: Power-efficient answer," *Nat. Photonics 2009 31*, vol. 3, pp. 27–29, 2009.

[64] S. G. Kipp, "Fibre Channel Connectivity Cabling Storage Area Networks," *fibrechannel.org*, 2016.

[65] T. Irujo, "Multimode or Single-Mode Optical Fiber?." `http://fiber-optic-catalog.ofsoptics.com/Asset/Multimode-or-Single-Mode.pdf`, 2017.

[66] B. E. A. Saleh and M. C. Teich, *Fundamentals of photonics*. Wiley Interscience, third ed., 2019.

[67] P. Pepeljugoski, S. Golowich, A. Ritger, P. Kolesar, and A. Risteski, "Modeling and simulation of next-generation multimode fiber links," *J. Light. Technol.*, vol. 21, no. 5, pp. 1242–1255, 2003.

[68] R. Olshansky, "Propagation in glass optical waveguides," *Rev. Mod. Phys.*, vol. 51, no. 2, pp. 341–367, 1979.

[69] Govind P. Agrawal, *Fiber Optic Communication Systems*. Wiley-Interscience, 3rd ed., 2002.

[70] M. J. Li and D. A. Nolan, "Optical transmission fiber design evolution," *J. Light. Technol.*, vol. 26, no. 9, pp. 1079–1092, 2008.

[71] "www.iso.org."

[72] ITU-T, "G.651.1 : Characteristics of a 50/125 μm multimode graded index optical fibre cable for the optical access network," tech. rep., 2018.

[73] T. Huynh, F. Doany, D. Kuchta, D. Gazula, E. Shaw, J. O'Daniel, and J. Tatum, "4x50Gb/s Shortwave-Wavelength Division Multiplexing VCSEL Link over 50m Multimode Fiber," in *2017 Opt. Fiber Commun. Conf. Exhib.*, vol. Tu2B.5., (Los Angeles, CA, USA), 2017.

[74] Y. Sun, R. Lingle, R. Shubochkin, K. Balemarthy, D. Braganza, T. Gray, W. J. Fan, and K. Wade, "51.56 Gb/ s SWDM PAM4 Transmission over Next Generation Wide Band Multimode Optical Fiber," *2016 Opt. Fiber Commun. Conf.*, pp. 50–52, 2016.

[75] J. M. Castro, R. Pimpinella, B. Kose, Y. Huang, B. Lane, A. Amezcua-Correa, M. Bigot, D. Molin, and P. Sillard, "200m 2x50Gbps PAM-4 SWDM transmission over WideBand Multimode Fiber using VCSELs and pre-distortion signal," in *2016 Opt. Fiber Commun. Conf.*, p. Tu2G.2, 2016.

[76] J. Lavrencik, S. Varughese, V. A. Thomas, G. Landry, Y. Sun, R. Shubochkin, K. Balemarthy, J. Tatum, and S. E. Ralph, "2λ x 100Gbps PAM-4 wideband fiber 100m links using 850nm and 940nm VCSELs," *2016 IEEE Photonics Conf. IPC 2016*, no. 1, pp. 751–752, 2017.

[77] Corning Inc., "Corning® ClearCurve® OM5 Wide Band Multimode Optical Fiber," 2017.

[78] L. OFS Fitel, "LaserWave® FLEX Wideband Optical Fiber."

[79] M.-J. Li, "MMF for High Data Rate and Short Length Applications," in *Opt. Fiber Commun. Conf.*, (Washington, D.C.), p. M3F.1, OSA, 2014.

[80] E. Simpanen, J. S. Gustavsson, A. Larsson, W. V. Sorin, S. Mathai, M. Tan, and S. Bickham, "Long-Reach 1060 nm SM VCSEL - SMF Optical Interconnects," in *2018 Eur. Conf. Opt. Commun.*, pp. 1–3, 2018.

[81] D. J. Richardson, J. M. Fini, and L. E. Nelson, "Space-division multiplexing in optical fibres," *Nat. Photonics 2013 75*, vol. 7, no. 5, p. 354, 2013.

[82] Anders Larsson, Johan S. Gustavsson, Petter Westbergh, Emanuel Haglund, Erik Haglund, Ewa Simpanen, E. Verband der Elektrotechnik, and Institute of Electrical and Electronics Engineers., "High-Speed VCSELs for Datacom," in *2016 Eur. Conf. Opt. Commun.*, 2016.

[83] P. Westbergh, J. S. Gustavsson, and A. Larsson, "VCSEL Arrays for Multicore Fiber Interconnects With an Aggregate Capacity of 240 Gb/s," *IEEE Photonics Technol. Lett.*, vol. 27, no. 3, pp. 296–299, 2015.

[84] J. Van Kerrebrouck, X. Pang, O. Ozolins, R. Lin, A. Udalcovs, L. Zhang, H. Li, S. Spiga, M. C. Amann, L. Gan, M. Tang, S. Fu, R. Schatz, G. Jacobsen, S. Popov, D. Liu, W. Tong, G. Torfs, J. Bauwelinck, J. Chen, and

X. Yin, “High-speed PAM4-based Optical SDM Interconnects with Directly Modulated Long-wavelength VCSEL,” *J. Light. Technol.*, vol. 37, no. 2, pp. 356–362, 2018.

[85] A. Valle and L. Pesquera, “Relative Intensity Noise of Multitransverse-Mode Vertical-Cavity Surface-Emitting Lasers,” *IEEE Photon. Technol. Lett.*, vol. 13, no. 4, pp. 272–274, 2001.

[86] D. M. Kuchta, A. V. Rylyakov, C. L. Schow, J. E. Proesel, C. W. Baks, P. Westbergh, J. S. Gustavsson, and A. Larsson, “A 50 Gb/s NRZ Modulated 850 nm VCSEL Transmitter Operating Error Free to 90 °C,” *J. Light. Technol.*, vol. 33, no. 4, pp. 802–810, 2015.

[87] G. Larisch and D. Bimberg, “How can we accommodate the rapidly increasing power consumption of the internet? "Green" optical interconnects based on novel VCSELs,” in *2017 19th Int. Conf. Transparent Opt. Networks*, IEEE, 2017.

[88] M. Ko, A. C. Ulusoy, and D. Kissinger, “A low-power VCSEL driver in a complementary SiGe:C BiCMOS technology,” in *2018 IEEE 18th Top. Meet. Silicon Monolith. Integr. Circuits RF Syst.*, pp. 45–47, 2018.

[89] M. Shibata and A. C. Carusone, “A 26-Gb/s 1.80-pJ/b CMOS-Driven Transmitter for 850-nm Common-Cathode VCSELs,” in *2015 Opt. Fiber Commun. Conf.*, p. Tu3G.1, 2015.

[90] B. Sedighi and J. Christoph Scheytt, “40 Gb/s VCSEL driver IC with a new output current and pre-emphasis adjustment method,” in *2012 IEEE/MTT-S Int. Microw. Symp. Dig.*, 2012.

[91] G. Belfiore, R. Henker, and F. Ellinger, “The effect of strong equalization in high-speed VCSEL-based optical communications up to 48 Gbit/s,” in *2016 IEEE Bipolar/BiCMOS Circuits Technol. Meet.*, pp. 13–16, IEEE, 2016.

[92] L. Szilagyi, G. Belfiore, R. Henker, and F. Ellinger, “30 Gbit/s 1.7 pJ/bit common-cathode tunable 850-nm-VCSEL driver in 28 nm digital CMOS,” in *2017 IEEE Opt. Interconnects Conf.*, pp. 51–52, 2017.

[93] J. Proesel, Z. Deniz, A. Cevrero, I. Ozkaya, S. Kim, D. Kuchta, S. Lee, S. Rylov, H. Ainspan, T. Dickson, J. Bulzacchelli, and M. Meghelli, “A 32Gb/s, 4.7pJ/bit optical link with âˆ’11.7dBm sensitivity in 14nm FinFET CMOS,” in *2017 Symp. VLSI Circuits*, pp. C318–C319, 2017.

[94] C. E. Shannon, “A mathematical theory of communication,” *Bell Syst. Tech. J.*, vol. 27, no. 3, pp. 379–423, 1948.

[95] X. Chen, S. R. Bickham, J. S. Abbott, J. D. Coleman, and M.-J. Li, "Multimode Fibers for Data Centers," in *Handb. Opt. Fibers*, pp. 1–57, Singapore: Springer Singapore, 2018.

[96] J. G. Proakis, *Digital Communications*. McGrawHill, 4th ed., 2008.

[97] S. Walklin and J. Conradi, "Multilevel signaling for increasing the reach of 10 Gb/s lightwave systems," *J. Light. Technol.*, vol. 17, no. 11, pp. 2235–2248, 1999.

[98] J. Gimlett and N.Cheung, "Dispersion penalty analysis for LED/single-mode fiber transmission systems," *J. Light. Technol.*, vol. 4, no. 9, pp. 1381–1392, 1986.

[99] D. Cunningham, M.Nowell, D. Hanson, and L. Kazovsky, "The IEEE 802.3z Worst Case Link Model for Optical Physical Media Dependent Specification." `http://www.ieee802.org/3/z/public/presentations/mar1997/DCwpaper.pdf`, 1997.

[100] K. Szczerba, P. Westbergh, J. Karout, J. S. Gustavsson, Å. Haglund, M. Karlsson, P. A. Andrekson, E. Agrell, and A. Larsson, "4-PAM for high-speed short-range optical communications," *IEEE/OSA J. Opt. Commun. Netw*, vol. 4, no. 11, pp. 885–894, 2012.

[101] P. Mecklenburg, W. K. Pehlert, and D. D. Sullivan, "Correction of Errors in Multilevel Gray-Coded Data," *IEEE Trans. Inf. Theory*, vol. 19, no. 3, pp. 336–340, 1973.

[102] J. K. Pollard, "Multilevel data communication over optical fibre," in *IEE Proc.-Commun*, vol. 138, pp. 162–168, 1991.

[103] J. Lavrencik, V. A. Thomas, S. Varughese, S. E. Ralph, and S. Member, "DSP-Enabled 100 Gb / s PAM-4 VCSEL MMF Links," *J. Light. Technol.*, vol. 35, no. 15, pp. 3189–3196, 2017.

[104] Marcus Müller, Ransom Stephens, and Russ McHugh, *Total Jitter Measurement at Low Probability Levels, Using Optimized BERT Scan Method*. Agilent Technologies, 2005.

[105] R. W. Hamming, "Error Detecting and Error Correcting Codes," *Bell Syst. Tech. J.*, vol. 29, no. 2, pp. 147–160, 1950.

[106] "InfiniBandâ„¢ Architecture Specification Volume 2 Release 1.3.1," 2012.

[107] "IEEE P802.3bm 40 Gb/s and 100 Gb/s Fiber Optic Task Force." `http://www.ieee802.org/3/bm/`.

[108] F. Karinou, N. Stojanovic, C. Prodaniuc, Z. Qiang, and T. Dippon, "112 Gb/s PAM-4 Optical Signal Transmission over 100-m OM4 Multimode Fiber for High-Capacity Data-Center Interconnects," *2016 Eur. Conf. Opt. Commun.*, pp. 124–126, 2016.

[109] K. Szczerba, P. Westbergh, M. Karlsson, P. A. Andrekson, and A. Larsson, "70 Gbps 4-PAM and 56 Gbps 8-PAM Using an 850 nm VCSEL," *J. Light. Technol.*, vol. 33, no. 7, pp. 1395–1401, 2015.

[110] N. Eiselt, H. Griesser, J. Wei, A. Dochhan, R. Hohenleitner, M. Ortsiefer, M. Eiselt, C. Neumeyr, J. J. V. Olmos, and I. T. Monroy, "Experimental Demonstration of 56 Gbit/s PAM-4 over 15 km and 84 Gbit/s PAM-4 over 1 km SSMF at 1525 nm using a 25G VCSEL," in *2016 Eur. Conf. Opt. Commun.*, 2016.

[111] S. K. Pavan, J. Lavrencik, and S. E. Ralph, "Experimental demonstration of 51.56 Gbit/s PAM-4 at 905nm and impact of level dependent RIN," in *2014 Eur. Conf. Opt. Commun.*, IEEE, 2014.

[112] S. K. Pavan, J. Lavrencik, R. Shubochkin, Y. Sun, J. Kim, D. S. Vaidya, R. Lingle, T. Kise, and S. Ralph, "50Gbit/s PAM-4 MMF Transmission Using 1060nm VCSELs with Reach beyond 200m," in *2014 Opt. Fiber Commun. Conf.*, p. W1F.5, 2014.

[113] J. M. Castro, R. Pimpinella, B. Kose, Y. Huang, B. Lane, K. Szczerba, P. Westbergh, T. Lengyel, J. S. Gustavsson, A. Larsson, and P. A. Andrekson, "48.7-Gb/s 4-PAM Transmission Over 200 m of High Bandwidth MMF Using an 850-nm VCSEL," *IEEE Photonics Technol. Lett.*, vol. 27, no. 17, pp. 1799–1801, 2015.

[114] C. Xie, S. Spiga, P. Dong, P. Winzer, M. Bergmann, B. Kogel, C. Neumeyr, and M.-C. Amann, "400-Gb/s PDM-4PAM WDM System Using a Monolithic 2x4 VCSEL Array and Coherent Detection," *J. Light. Technol.*, vol. 33, no. 3, pp. 670–677, 2015.

[115] C. Xie, P. Dong, P. Winzer, C. Gréus, M. Ortsiefer, C. Neumeyr, S. Spiga, M. Müller, and M.-C. Amann, "960-km SSMF transmission of 1057-Gb/s PDM 3-PAM using directly modulated VCSELs and coherent detection," *Opt. Express*, vol. 21, no. 9, p. 11585, 2013.

[116] D. M. Kuchta, A. Rylyakov, C. Schow, J. Proesel, F. Doany, C. W. Baks, B. Hamel-Bissell, C. Kocot, L. Graham, R. Johnson, G. Landry, E. Shaw, A. MacInnes, and J. Tatum, "A 56.1Gb/s NRZ Modulated 850nm VCSEL-Based Optical Link," in *2013 Opt. Fiber Commun. Conf. Expo. Natl. Fiber Opt. Eng. Conf.*, p. OW1B.5, 2013.

[117] C. Xie, P. Dong, S. Randel, D. Pilori, P. Winzer, S. Spiga, B. Kögel, C. Neumeyr, and M. C. Amann, "Single-VCSEL 100-Gb/s short-reach system using discrete multi-tone modulation and direct detection," in *2015 Opt. Fiber Commun. Conf.*, 2015.

[118] M. Liu, C. Y. Wang, M. Feng, and N. Holonyak, "50 Gb / s Error-Free Data Transmission of 850 nm Oxide-confined VCSELs," in *2016 2015 Opt. Fiber Commun. Conf.*, pp. 98–100, 2016.

[119] A. Dochhan, N. Eiselt, R. Hohenleitner, H. Griesser, M. Eiselt, M. Ortsiefer, C. Neumeyr, J. J. Vegas Olmos, I. Tafur Monroy, and J.-P. Elbers, "56 Gb/s DMT Transmission with VCSELs in 1.5 um Wavelength Range over up to 12 km for DWDM Intra-Data Center Connects," *2016 Eur. Conf. Opt. Commun.*, no. 1, pp. 391–393, 2016.

[120] R. Safaisini, E. Haglund, A. Larsson, J. Gustavsson, E. Haglund, and P. Westbergh, "High-speed 850 nm VCSELs operating error free up to 57 Gbit/s," *Electron. Lett.*, vol. 49, no. 16, pp. 1021–1023, 2013.

[121] D. M. Kuchta, T. N. Huynh, F. E. Doany, L. Schares, C. W. Baks, C. Neumeyr, A. Daly, B. Kogel, J. Rosskopf, and M. Ortsiefer, "Error-Free 56 Gb/s NRZ Modulation of a 1530-nm VCSEL Link," *J. Light. Technol.*, vol. 34, no. 14, pp. 3275–3282, 2016.

[122] D. Bimberg, G. Larisch, H. Li, P. Moser, P. Wolf, and J. Lott, "Error-free 46 Gbit/s operation of oxide-confined 980 nm VCSELs at 85°C," *Electron. Lett.*, vol. 50, no. 19, pp. 1369–1371, 2014.

[123] D. M. Kuchta, A. V. Rylyakov, C. L. Schow, J. E. Proesel, C. W. Baks, P. Westbergh, J. S. Gustavsson, and A. Larsson, "A 50 Gb/s NRZ Modulated 850 nm VCSEL Transmitter Operating Error Free to 90 °C," *J. Light. Technol.*, vol. 33, no. 4, pp. 802–810, 2015.

[124] D. Kuchta, A. V. Rylyakov, C. L. Schow, J. Proesel, C. Baks, P. Westbergh, J. S. Gustavsson, and A. Larsson, "64Gb/s Transmission over 57m MMF using an NRZ Modulated 850nm VCSEL," in *2014 Opt. Fiber Commun. Conf.*, p. Th3C.2, 2014.

[125] I. Lyubomirsky, W. A. Ling, R. Rodes, H. M. Daghighian, and C. Kocot, "56 Gb/s transmission over 100m OM3 using 25G-class VCSEL and discrete multi-tone modulation," in *2014 Opt. Interconnects Conf.*, pp. 85–86, 2014.

[126] W. Ling, I. Lyubomirsky, R. Rodes, H. Daghighian, and C. Kocot, "Single-Channel 50G and 100G Discrete Multitone Transmission With

25G VCSEL Technology," *J. Light. Technol.*, vol. 33, no. 4, pp. 761–767, 2015.

[127] I. C. Lu, C. C. Wei, H. Y. Chen, K. Z. Chen, C. H. Huang, K. L. Chi, J. W. Shi, F. I. Lai, D. H. Hsieh, H. C. Kuo, W. Lin, S. W. Chiu, and J. Chen, "Very High Bit-Rate Distance Product Using High-Power Single-Mode 850-nm VCSEL With Discrete Multitone Modulation Formats Through OM4 Multimode Fiber," *IEEE J. Sel. Top. Quantum Electron.*, vol. 21, no. 6, pp. 444–452, 2015.

[128] K. Szczerba, P. Westbergh, M. Karlsson, A. Larsson, and P. Andrekson, "60 Gbits error-free 4-PAM operation with 850 nm VCSEL," *Electron. Lett.*, vol. 49, no. 15, pp. 953–955, 2013.

[129] P. Moser, J. Lott, P. Wolf, G. Larisch, H. Li, and D. Bimberg, "Temperature-Stable Oxide-Confined 980 nm VCSELs Operating Error-Free at 46 Gb/s and 85°C," in *2014 Int. Semicond. Laser Conf.*, pp. 76–77, 2014.

[130] H. Li, P. Wolf, P. Moser, S. Member, G. Larisch, J. A. Lott, S. Member, and D. Bimberg, "Temperature-Stable, Energy-Efficient, and High-Bit Rate Oxide-Confined 980-nm VCSELs for Optical Interconnects," *IEEE J. Sel. Top. Quantum Electron.*, vol. 21, no. 6, 2015.

[131] H. Li, J. Lott, P. Wolf, D. Bimberg, D. Arsenijević, and P. Moser, "40 Gbit/s data transmission with 980 nm VCSELs at 120°C using four-level pulse-amplitude modulation," *Electron. Lett.*, vol. 51, no. 19, pp. 1517–1519, 2015.

[132] E. Simpanen, J. S. Gustavsson, E. P. Haglund, E. P. Haglund, A. Larsson, W. V. Sorin, S. Mathai, and M. Tan, "1060 nm VCSEL for up to 40 Gbit/s Data Transmission," in *Int. Semicond. Laser Conf.*, pp. 2–3, 2016.

[133] S. Kota Pavan, J. Lavrencik, R. Shubochkin, Y. Sun, J. Kim, D. S. Vaidya, R. Lingle, T. Kise, and S. Ralph, "50Gbit/s PAM-4 MMF Transmission Using 1060nm VCSELs with Reach beyond 200m," in *2014 Opt. Fiber Commun. Conf.*, p. W1F.5, 2014.

[134] I. P. Kaminow, T. Li, and A. E. Willner, *Optical fiber telecommunications VI. A, Components and subsystems.* Academic Press, 2013.

[135] C. Kottke, C. Caspar, V. Jungnickel, R. Freund, M. Agustin, J. R. Kropp, and N. N. Ledentsov, "High-Speed DMT and VCSEL-Based MMF Transmission Using Pre-Distortion," *J. Light. Technol.*, vol. 36, no. 2, pp. 168–174, 2018.

[136] K. Szczerba, P. Westbergh, J. S. Gustavsson, M. Karlsson, P. A. Andrekson, and A. Larsson, "Energy Efficiency of VCSELs in the Context of Short-Range Optical Links," *IEEE Photonics Technol. Lett.*, vol. 27, no. 16, pp. 1749–1752, 2015.

[137] D. D. Falconer, "Carrierless AM/PM," *Bell Lab. Tech. Memo.*, no. Tech. Rep., 1970.

[138] M. B. Othman, Xu Zhang, Lei Deng, M. Wieckowski, J. B. Jensen, and I. T. Monroy, "Experimental Investigations of 3-D-/4-D-CAP Modulation With Directly Modulated VCSELs," *IEEE Photonics Technol. Lett.*, vol. 24, no. 22, pp. 2009–2012, 2012.

[139] X. Lu, D. Zibar, and I. T. Monroy, "24-Dimensional Rate-Flexible Carrierless and Amplitude Phase Modulation for 100G IM-DD Transmission Using 850nm VCSEL," in *2018 Eur. Conf. Opt. Commun.*, 2018.

[140] M. I. Olmedo, T. Zuo, J. B. Jensen, Q. Zhong, X. Xu, S. Popov, and I. T. Monroy, "Multiband Carrierless Amplitude Phase Modulation for High Capacity Optical Data Links," *J. Light. Technol.*, vol. 32, no. 4, pp. 798–804, 2014.

[141] R. Puerta, J. J. V. Olmos, I. T. Monroy, N. N. Ledentsov, and J. P. Turkiewicz, "Flexible MultiCAP Modulation and its Application to 850 nm VCSEL-MMF Links," *J. Light. Technol.*, vol. 35, no. 15, pp. 3168–3173, 2017.

[142] C. Xie, S. Spiga, P. Dong, P. Winzer, M. Bergmann, B. Kogel, C. Neumeyr, and M.-C. Amann, "400-Gb/s PDM-4PAM WDM System Using a Monolithic 2Ã—4 VCSEL Array and Coherent Detection," *J. Light. Technol.*, vol. 33, no. 3, pp. 670–677, 2015.

[143] J. B. Jensen, R. Rodes, A. Caballero, N. Cheng, D. Zibar, and I. T. Monroy, "VCSEL Based Coherent PONs," *J. Light. Technol.*, vol. 32, no. 8, pp. 1423–1433, 2014.

[144] "Most Power Consumed (MW) : World's Top Data Centers." `http://worldstopdatacenters.com/power/`.

[145] H. Rong, H. Zhang, S. Xiao, C. Li, and C. Hu, "Optimizing energy consumption for data centers," *Renew. Sustain. Energy Rev.*, vol. 58, pp. 674–691, 2016.

[146] J. Lavrencik, S. Varughese, V. A. Thomas, and S. E. Ralph, "Scaling VCSEL-MMF Links to 1 Tb/s Using Short Wavelength Division Multiplexing," *J. Light. Technol.*, vol. 36, no. 18, pp. 4138–4145, 2018.

[147] T. Liljeberg, "Silicon photonics and the future of optical connectivity in the data center," in *2017 IEEE Opt. Interconnects Conf.*, pp. 1–2, 2017.

[148] A. L. G. Roelkens, E. P. Haglund, S. Kumari , E. Haglund, J. S. Gustavsson, R. Baets, "850 nm hybrid vertical cavity laser integration for on-chip silicon photonics light sources," in *2017 Opt. Fiber Commun. Conf. Exhib.*, (Los Angeles, CA, USA), 2017.

[149] E. P. Haglund, S. Kumari, P. Westbergh, J. S. Gustavsson, R. G. Baets, G. Roelkens, and A. Larsson, "20-Gb/s Modulation of Silicon-Integrated Short-Wavelength Hybrid-Cavity VCSELs," *IEEE Photonics Technol. Lett.*, vol. 28, no. 8, pp. 856–859, 2016.

[150] X. Wen, Z. Ruan, Y. Zhu, X. Cai, P. Chen, and L. Liu, "Integration of vertical-cavity surface-emitting laser on silicon photonic circuits using tilted membrane based grating couplers," in *2018 Asia Commun. Photonics Conf.*, pp. 1–3, 2018.

[151] J. Verbist, M. Verplaetse, S. A. Srinivasan, P. De Heyn, T. De Keulenaer, R. Vaernewyck, R. Pierco, A. Vyncke, P. Verheyen, S. Balakrishnan, G. Lepage, M. Pantouvaki, P. Absil, X. Yin, G. Roelkens, G. Torfs, J. Van Campenhout, and J. Bauwelinck, "Real-time 100 Gb/s NRZ-OOK transmission with a silicon photonics GeSi electro-absorption modulator," in *2017 IEEE Opt. Interconnects Conf.*, pp. 29–30, 2017.

[152] Y.-K. C. P. Dong, X. Liu, S. Chandrasekhar, L. L. Buhl, R. Aroca, Y. Baeyens, "224-Gb/s PDM-16-QAM modulator and receiver based on silicon photonic integrated circuits," in *2013 Opt. Fiber Commun. Conf. Expo. Natl. Fiber Opt. Eng. Conf.*, (Anaheim, CA, USA), 2013.

[153] T. Shi, T.-I. Su, N. Zhang, C.-Y. Hong, and D. Pan, "Silicon Photonics Platform for 400G Data Center Applications," in *2018 Opt. Fiber Commun. Conf. Expo.*, 2018.